Supplementary Information for

Exploring Cellular Gateways: Unraveling the Secrets of Disordered Proteins within Live Nuclear Pores

Wenaln Yu, Mark Tingey, Joseph M. Kelich, Yichen Li, Jingjie Yu, Samuel L. Junod, Zecheng Jiang, Ian Hansen, Nacef Good, and Weidong Yang*

Affiliations: Department of Biology, Temple University, Philadelphia, Pennsylvania, USA
*** Corresponding author:** Prof. Weidong Yang, Email: weidong.yang@temple.edu; Tel: 215-204-2312.

Supplementary information includes:

Methods (additional)

Table S1-S8

Figure S1- S19

Movie S1-S21

Methods (additional)

Cell Culture and Transport Conditions for Single-Molecule Experiments in Permeabilized Cells A stable HeLa cell line expressing the GFP-conjugate of POM121 was utilized in this study. Freshly split cells were cultivated overnight on coverslips in DMEM supplemented with 10% FBS. Microscopy experiments were conducted using custom-made flow chambers, comprising a top cover-slip separated by two lines of silicone grease spacers. Prior to imaging, cells were rinsed with transport buffer (20 mM HEPES, 110 mM KOAc, 5 mM NaOAc, 2 mM MgOAc, 1 mM EGTA, pH 7.3), permeabilized for two minutes with 40 µg/mL digitonin in transport buffer, and then washed again with transport buffer containing 1.5% polyvinylpyrrolidone (PVP; 360 kDa). The inclusion of PVP in all transport buffer solutions after digitonin treatment aimed to prevent osmotic swelling of the nuclei. For single-molecule measurements of transport receptors and the passive diffusion of various molecules, 1 nM intrinsic fluorescent or dye-labeled substrates were used. Further experimental details can be found in previously published methods[5-10].

Dyes, Dextran, Proteins, and Labeling in Permeabilized Cells Fluorescein, Alexa Fluor 647, and dye-labeled dextrans were procured from Invitrogen, while insulin and α-lactalbumin were obtained from Sigma-Aldrich. N-terminal His-tagged GFP, NTF2, Imp β1, and transportin proteins were expressed in Escherichia coli and purified through Ni-NTA Superflow (Qiagen), MonoQ, and Superdex 200 (Amersham) chromatography.

The model substrate NLS-2xGFP and other transport cofactors were purified as described in previous reports[5-10]. The solvent-accessible cysteines on the proteins were labeled with a 20-fold molar excess of Alexa Fluor 647 maleimide dye (Invitrogen) for 2 hours at room temperature in 50 mM sodium phosphate, 150 mM NaCl, pH 7.5. Reactions were quenched with β-mercaptoethanol, and the labeled products were dialyzed to remove free dyes. The labeling ratio comprised 1 dye per protein molecule for GFP, NTF2, insulin, and α-lactalbumin; 2 dyes per transportin molecule; and 4 dyes per protein molecule for Imp β1 and NLS-2xGFP.

Table S1. The transit time and efficiency of free JFdye, and unbound Nup153, passing through the NPC.

Particle	Nuclear transport time (ms)	Import efficiency (%)	Export efficiency (%)	Detection frame rate (ms)
Free JF646	3 ± 1	-48 ± 2	-48 ± 2	2
GFP-Nup153	11 ± 8	58 ± 6	26 ± 5	2

Table S2. Single-molecule localization precision, number of points, and reproducibility used to generate 3D probability density maps for each FG-Nups

Nup	Terminal	Single molecule precision (nm)	X-axis region (nm)	Bin Size	R position (nm)	# of points	Reproducibility (%)
Nup358	N	8.4	[-111.0,-78.0]	7.75	17 (40.42%) 61 (59.58%)	204	83 93
			[-78.0,-63.0]	10.55	28	207	98
			[-63.0,-53.0]	9.50	23	219	97
			[-53.0,-43.0]	10.20	23	214	98
			[-43.0,-34.0]	8.75	17	209	93
			[-34.0,-20.0]	8.60	22	215	98
			[-20.0,22.0]	8.85	22	200	97
	C (FG)	8.8	[-114.0,-85.0]	5.75	11	200	100
			[-85.0,-61.0]	8.85	13	208	75
			[-61.0,-37.0]	6.85	15	204	82
			[-37.0,3.0]	7.70	23	200	97
Nup214	N	8.4	[-152, -117.0]	9.00	55	200	98
			[-117.0, -100.0]	7.85	18	203	93
			[-100.0,-86.0]	9.30	25	201	98
			[-86.0,-74.0]	8.95	53	200	99
			[-74.0,-62.0]	9.90	40	222	99
			[-62.0,-52.0]	9.55	53	202	99
			[-52.0,-38.0]	8.45	29	211	97
			[-38.0,-22.0]	11.70	52	203	98
			[-22.0,19.0]	6.75	21	201	97
	C (FG)	7.3	[-107.0,-82.0]	4.45	9	204	100
			[-82.0,-58.0]	8.50	0	204	100
			[-58.0,-35.0]	5.40	21	206	97
			[-35.0,29.0]	10.10	30	200	99
hCG1	N (FG)	6.5	[-149.0,-110.0]	4.00	15	202	92

			[-110.0,-76.0]	7.60	22	206	97
			[-76.0,-38.0]	7.25	9	201	100
			[-38.0,-10.0]	6.20	18	107	92
			[-10.0, 42.0]	8.20	8	100	99
	C (FG)	7.7	[-106.0,-76.0]	4.25	27	202	97
			[-76.0,-60.0]	4.25	19	204	95
			[-60.0,-44.0]	7.55	10	213	100
			[-44.0,-28.0]	5.00	17	206	92
			[-28.0,-2.0]	9.15	18	202	95

Nup	**Terminal**	**Single molecule precision (nm)**	**X-axis region (nm)**	**Bin Size**	**3D peak fit position (nm)**	**# of points**	**Reproducibility (%)**
Nup98	N (FG)	6.5	[-93.0,-63.0]	4.20	12 (40.73%) 59 (59.27%)	203	73 92
			[-63.0,-43.0]	5.85	14 (41.48%) 59 (58.52%)	201	79 92
			[-43.0,-20.0]	5.90	7	291	100
			[-20.0,20.0]	5.45	18	462	99
			[20.0,41.0]	10.55	34	295	100
			[41.0,60.0]	8.65	51	204	99
			[60.0,83.0]	10.05	53	212	99
			[83.0,115.0]	8.75	30 (81.65%) 95 (18.35%)	201	98 54
	C	6.8	[-46.0,-30.0]	6.75	24	204	98
			[-30.0,-20.0]	4.10	22	201	98
			[-20.0,-13.0]	6.65	14	205	90
			[-13.0,-5.0]	4.20	15	221	94
			[-5.0,5.0]	4.65	18	241	96
			[5.0,13.0]	4.20	17	208	96
			[13.0,21.0]	6.95	18	205	96
			[21.0,30.0]	8.50	28	206	99
			[30.0,44.0]	4.95	24	200	93
Nup62	N (FG)	8.2	[-23.0,20.0]	4.00	16	327	92
	C	7.2	[-20.0,20]	4.50	19	212	97
Nup54	N (FG)	6.3	[-35.0,19.0]	5.25	21	204	98
	C	6.3	[-20,20]	10.05	20	206	98
POM121	N	7.2	[-49.0,-23.0]	11.60	43	202	99
			[-23.0,-7.0]	7.60	48	203	99
			[-7.0,9.0]	7.40	43	221	99

			[9.0,27.0]	11.10	40	205	98
			[27.0,57.0]	12.00	52	202	99
	C (FG)	8.1	[-47.0,-15.0]	4.05	18	200	93
			[-15.0,-5.0]	6.05	20	200	93
			[-5.0,5.0]	8.80	17	214	91
			[5.0,15.0]	10.85	25	205	97
			[15.0,42.0]	4.70	9	201	100
Nup58	N (FG)	8	[-22.0,3.0]	4.05	17	203	92
			[3.0,19.0]	5.75	17	210	92
			[19.0,43.0]	8.45	17	200	93
Nup58	C (FG)	6.2	[-58.0,-30.0]	7.15	14	202	95
			[-30.0,-11.0]	8.90	18	203	97
			[-11.0,9.0]	6.15	23	210	99
			[9.0,28.0]	7.00	21	202	98
			[28.0,61.0]	9.95	18	208	98

Nup	Terminal	Single molecule precision (nm)	X-axis region (nm)	Bin Size	3D peak fit position (nm)	# of points	Reproducibility (%)
Nup50	N (FG)	8.9	[-18.0,17.0]	6.75	22	205	96
			[17.0,32.0]	5.65	20	205	95
			[32.0,46.0]	4.45	20	213	94
			[46.0,64.0]	5.05	13	205	94
			[64.0,99.0]	10.80	0	203	86
	C	7.9	[-86.0,10.0]	9.65	26	200	96
			[10.0,33.0]	11.05	31	206	99
			[33.0,53.0]	7.70	24	211	98
			[53.0,78.0]	11.85	22	204	96
			[78.0,149.0]	10.20	10	201	100
Nup153	N	6.1	[12.0,25.0]	4.75	13	202	90
			[25.0,39.0]	9.60	18	231	99
			[39.0,59.0]	10.05	18 (54.56%) 50 (45.44%)	203	98 81
			[59.0,116.0]	6.25	4 (21.22%) 18 (78.78%)	201	97 97
	C (FG)	8.7	[-10.0,22.0]	5.30	18	202	91
			[22.0,44.0]	4.70	7	200	99
			[44.0,64.0]	6.70	37	207	99
			[64.0,89.0]	8.65	23	200	95
			[89.0,125.0]	4.00	0	201	85
TPR	N	9.2	[-28.0,23.0]	5.65	25	200	98
			[23.0,39.0]	9.95	29	205	99

			[39.0,78.0]	10.35	29	200	95
	C (FG)	9.4	[-7.0,40.0]	4.50	32	201	98
			[40.0,68.0]	7.00	20 (20.52%) 49 (79.48%)	217	94 99
			[68.0,113.0]	5.05	16	203	86

Table S3. Correlation map for the following Tables S4-S6. Presented here is a color-coded map, accompanied by the associated numerical scores that assess the correlation between different Nups. The color code used in the subsequent tables is also provided for reference [1].

Correlation coefficient	Interpretation
0.90 to 1.00	Very high positive correlation
0.70 to 0.90	High positive correlation
0.50 to 0.70	Moderate positive correlation
0.30 to 0.50	Low positive correlation
-0.30 to 0.30	Negligible correlation
-0.50 to -0.30	Low negative correlation
-0.70 to -0.50	Moderate negative correlation
-0.90 to -0.70	High negative correlation
-1.00 to -0.90	Very high negative correlation

Table S4. Spearman's rank correlation coefficient on X dimension. Spearman's rank correlation coefficients for X-dimensional data across all FG-Nups are presented. The Nups are categorized based on their localization within the NPC and are compared to all other Nups. For a comprehensive understanding of the positive or negative correlation, please refer to Table S3 for the color code and numerical interpretations.

	Nup358C	Nup214C	hCG1N	hCG1C	POM121C	Nup98N	Nup58N	Nup58C	Nup62N	Nup54N	TPRC	Nup153C	Nup50N
Nup358C	1.000	0.987	0.933	0.829	-0.006	0.038	-0.210	0.061	0.146	0.052	-0.529	-0.459	-0.442
Nup214C	0.987	1.000	0.900	0.866	-0.103	0.060	-0.303	0.065	0.062	-0.029	-0.580	-0.474	-0.504
hCG1N	0.933	0.900	1.000	0.751	-0.071	-0.102	-0.271	-0.071	0.091	0.008	-0.532	-0.488	-0.467
hCG1C	0.829	0.866	0.751	1.000	-0.022	0.240	-0.266	0.264	0.196	0.094	-0.565	-0.400	-0.483
POM121C	-0.006	-0.103	-0.071	-0.022	1.000	0.928	0.699	1.000	0.853	0.955	-0.119	0.253	0.129
Nup98N	0.038	0.060	-0.102	0.240	0.928	1.000	0.972	0.928	0.828	0.884	0.543	0.549	0.771
Nup58N	-0.210	-0.303	-0.271	-0.266	0.699	0.972	1.000	0.881	0.433	0.560	0.224	0.481	0.556
Nup58C	0.061	0.065	-0.071	0.264	1.000	0.928	0.881	1.000	0.947	0.986	0.138	0.268	0.408
Nup62N	0.146	0.062	0.091	0.196	0.853	0.828	0.433	0.947	1.000	0.958	-0.266	0.052	-0.063
Nup54N	0.052	-0.029	0.008	0.094	0.955	0.884	0.560	0.986	0.958	1.000	-0.200	0.146	0.025
TPRC	-0.529	-0.580	-0.532	-0.565	-0.119	0.543	0.224	0.138	-0.266	-0.200	1.000	1.000	0.821
Nup153C	-0.459	-0.474	-0.488	-0.400	0.253	0.549	0.481	0.268	0.052	0.146	1.000	1.000	0.897
Nup50N	-0.442	-0.504	-0.467	-0.483	0.129	0.771	0.556	0.408	-0.063	0.025	0.821	0.897	1.000

Table S5. Pearson correlation coefficient on X dimension. Pearson's correlation coefficients for X-dimensional data involving all FG repeat-containing Nups are provided. These Nups are categorized based on their localization within the NPC and compared to all other Nups. To better interpret positive or negative correlations, please consult Table S3 for the associated color code and numerical explanations.

	Nup358C	Nup214C	hCG1N	hCG1C	POM121C	Nup98N	Nup58N	Nup58C	Nup62N	Nup54N	TPRC	Nup153C	Nup50N
Nup358C	1.000	0.989	0.916	0.793	-0.306	0.044	-0.432	-0.032	-0.125	-0.159	-0.687	-0.618	-0.630
Nup214C	0.989	1.000	0.869	0.811	-0.410	0.019	-0.524	-0.094	-0.227	-0.259	-0.702	-0.649	-0.672
hCG1N	0.916	0.869	1.000	0.585	-0.278	-0.151	-0.416	-0.259	-0.148	-0.198	-0.629	-0.601	-0.634
hCG1C	0.793	0.811	0.585	1.000	-0.236	0.237	-0.382	0.168	0.075	0.013	-0.676	-0.567	-0.626
POM121C	-0.306	-0.410	-0.278	-0.236	1.000	0.590	0.813	0.838	0.803	0.891	-0.285	-0.018	0.000
Nup98N	0.044	0.019	-0.151	0.237	0.590	1.000	0.745	0.918	0.614	0.643	0.418	0.477	0.642
Nup58N	-0.432	-0.524	-0.416	-0.382	0.813	0.745	1.000	0.875	0.499	0.598	0.069	0.282	0.438
Nup58C	-0.032	-0.094	-0.259	0.168	0.838	0.918	0.875	1.000	0.847	0.884	0.083	0.252	0.364
Nup62N	-0.125	-0.227	-0.148	0.075	0.803	0.614	0.499	0.847	1.000	0.980	-0.432	-0.181	-0.221
Nup54N	-0.159	-0.259	-0.198	0.013	0.891	0.643	0.598	0.884	0.980	1.000	-0.418	-0.151	-0.175
TPRC	-0.687	-0.702	-0.629	-0.676	-0.285	0.418	0.069	0.083	-0.432	-0.418	1.000	0.977	0.839
Nup153C	-0.618	-0.649	-0.601	-0.567	-0.018	0.477	0.282	0.252	-0.181	-0.151	0.977	1.000	0.871
Nup50N	-0.630	-0.672	-0.634	-0.626	0.000	0.642	0.438	0.364	-0.221	-0.175	0.839	0.871	1.000

Table S6. Spearman's rank correlation coefficient on R dimension. Spearman's rank correlation coefficients for R-dimensional data involving all FG repeat-containing Nups are presented. These Nups are categorized based on their localization within the NPC and compared to all other Nups. To better understand positive or negative correlations, please refer to Table S3 for the associated color code and numerical explanations.

	Nup358C	Nup214C	hCG1N	hCG1C	POM121C	Nup98N	Nup58N	Nup58C	Nup62N	Nup54N	TPRC	Nup153C	Nup50N
Nup358C	1.000	0.688	0.664	0.853	0.720	0.720	0.678	0.678	0.678	0.678	0.533	0.741	0.678
Nup214C	0.688	1.000	0.442	0.758	0.609	0.609	0.521	0.521	0.521	0.521	0.763	0.675	0.521
hCG1N	0.664	0.442	1.000	0.636	0.262	0.262	0.405	0.405	0.405	0.405	0.566	0.367	0.405
hCG1C	0.853	0.758	0.636	1.000	0.879	0.879	0.806	0.806	0.806	0.806	0.626	0.903	0.806
POM121C	0.720	0.609	0.262	0.879	1.000	1.000	0.952	0.952	0.952	0.952	0.456	0.950	0.952
Nup98N	0.720	0.609	0.262	0.879	1.000	1.000	0.800	0.800	0.800	0.800	0.456	0.950	0.800
Nup58N	0.678	0.521	0.405	0.806	0.952	0.800	1.000	1.000	1.000	1.000	0.390	0.850	1.000
Nup58C	0.678	0.521	0.405	0.806	0.952	0.800	1.000	1.000	1.000	1.000	0.390	0.850	1.000
Nup62N	0.678	0.521	0.405	0.806	0.952	0.800	1.000	1.000	1.000	1.000	0.390	0.850	1.000
Nup54N	0.678	0.521	0.405	0.806	0.952	0.800	1.000	1.000	1.000	1.000	0.390	0.850	1.000
TPRC	0.533	0.763	0.566	0.626	0.456	0.456	0.390	0.390	0.390	0.390	1.000	0.555	0.390
Nup153C	0.741	0.675	0.367	0.903	0.950	0.950	0.850	0.850	0.850	0.850	0.555	1.000	0.850
Nup50N	0.678	0.521	0.405	0.806	0.952	0.800	1.000	1.000	1.000	1.000	0.390	0.850	1.000

Table S7. Pearson correlation coefficient on R dimension. Pearson's correlation coefficients for R-dimensional data involving all FG repeat-containing Nups are provided. These Nups are categorized based on their localization within the NPC and compared to all other Nups. For a comprehensive understanding of positive or negative correlations, please refer to Table S3 for the corresponding color codes and numerical explanations.

	Nup358C	Nup214C	hCG1N	hCG1C	POM121C	Nup98N	Nup58N	Nup58C	Nup62N	Nup54N	TPRC	Nup153C	Nup50N
Nup358C	1.000	0.786	0.657	0.901	0.737	0.821	0.791	0.809	0.812	0.814	0.427	0.739	0.684
Nup214C	0.786	1.000	0.204	0.776	0.523	0.631	0.450	0.505	0.429	0.526	0.715	0.579	0.342
hCG1N	0.657	0.204	1.000	0.414	0.286	0.250	0.511	0.447	0.552	0.422	0.189	0.416	0.497
hCG1C	0.901	0.776	0.414	1.000	0.773	0.928	0.804	0.843	0.831	0.856	0.339	0.775	0.685
POM121C	0.737	0.523	0.286	0.773	1.000	0.804	0.843	0.861	0.689	0.865	0.101	0.975	0.875
Nup98N	0.821	0.631	0.250	0.928	0.804	1.000	0.889	0.939	0.878	0.954	-0.018	0.726	0.743
Nup58N	0.791	0.450	0.511	0.804	0.843	0.889	1.000	0.991	0.954	0.983	-0.137	0.736	0.956
Nup58C	0.809	0.505	0.447	0.843	0.861	0.939	0.991	1.000	0.945	0.999	-0.103	0.761	0.917
Nup62N	0.812	0.429	0.552	0.831	0.689	0.878	0.954	0.945	1.000	0.938	-0.117	0.589	0.872
Nup54N	0.814	0.526	0.422	0.856	0.865	0.954	0.983	0.999	0.938	1.000	-0.089	0.768	0.897
TPRC	0.427	0.715	0.189	0.339	0.101	-0.018	-0.137	-0.103	-0.117	-0.089	1.000	0.273	-0.187
Nup153C	0.739	0.579	0.416	0.775	0.975	0.726	0.736	0.761	0.589	0.768	0.273	1.000	0.767
Nup50N	0.684	0.342	0.497	0.685	0.875	0.743	0.956	0.917	0.872	0.897	-0.187	0.767	1.000

Table S8. An overview of various models concerning the NPC[2], including the year of proposal if applicable, and a comparative analysis of distinct characteristics. The abbreviation "n/c" denotes "not clear".

Model (year)	**Single or multiple channels at the NPC's center for passive diffusion**	**Distinct passive and facilitated pathways through the NPC**	**FG Nups at the NPC's center or/and both ends contribute to the NPC's selectivity.**	**A plug or no plug within the center of NPC**
Plug 1982	Multiple	n/c	n/c	Yes
Gradient 2001	n/c	Yes	Center and both ends	n/c
Oily spaghetti 2001	Single	Yes	Center	No
Selective phase / hydrogel 2001	Multiple	No	Center	n/c
Virtual gating/Polymer brush 2003	Single	Yes	Both ends	No
ROD 2005	Single	Yes	Non-FG domains	No
Forest 2010	Multiple	Yes	Center and both ends	Yes
CATCH 2023	Single	Yes	Center and both ends	No

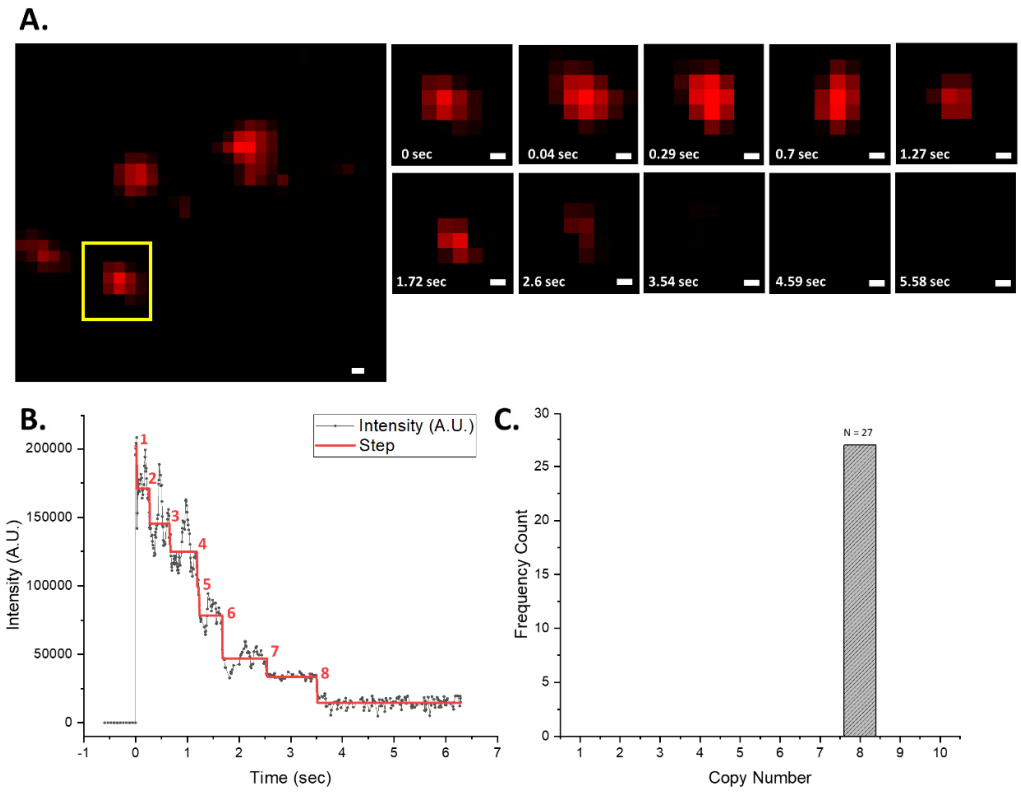

Figure S1. The quantity of Pom121 copies per NPC in live HeLa cells with stable expression of mCherry-POM121.

(A) This illustration showcases individual NPCs located at the bottom of the nuclear envelope. A single NPC is emphasized in yellow, accompanied by a time-series of that specific region of interest. Scale bar: 150 nm. (B) The integrated intensity of the highlighted NPC is presented here, reflecting the number of photobleaching steps it underwent. Each step corresponds to the photobleaching of a copy of mCherry-POM121. (C) The frequency count of NPCs was assessed to determine the number of photobleaching steps per NPC. Among the 27 NPCs scanned in 27 live cells, eight copies of mCherry-POM121 were confirmed.

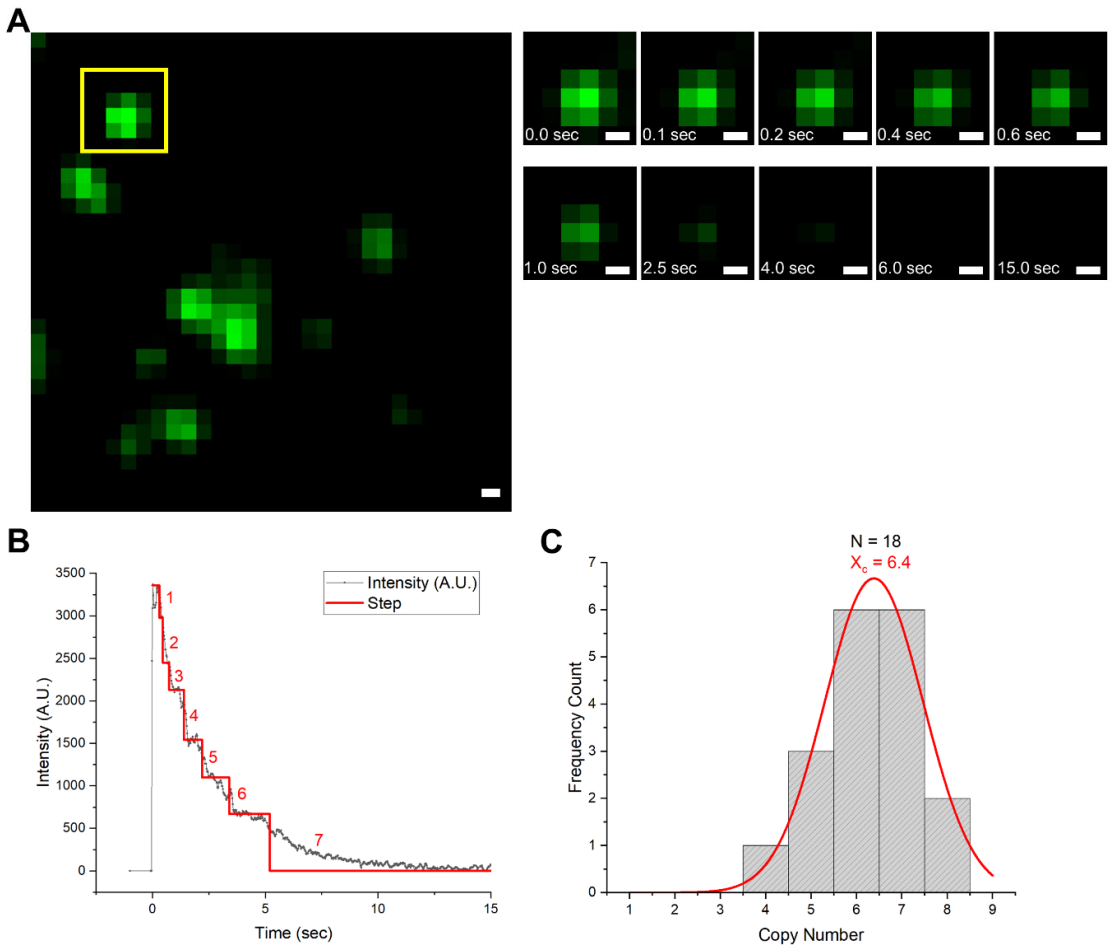

Figure S2. The number of Pom121 copies per NPC in live HeLa cells was determined following transient transfection of HaLo-Pom121-GFP.

(A) This panel displays individual NPCs located at the bottom of the nuclear envelope. A specific NPC is enclosed within a red box, accompanied by a time-series capturing changes in that region of interest. The beginning of the photobleaching process is marked at 0 seconds. The scale: 200 nm. (B) The integrated intensity of the highlighted NPC is depicted, which provides information about the number of photobleaching steps. (C) This panel presents the results of the frequency count analysis conducted on 18 NPCs in 18 different live cells, revealing that more than 90% of NPCs contain 5-8 copies of Halo-Pom121-GFP. Other FG Nups have undergone comparable measurements, indicating that over 60% of native FG Nups within each NPC have been substituted with labeled FG Nups. Supplementary Fig. S20 demonstrates that a comprehensive FG Nups map can be generated once the labeling ratio surpasses 50%, employing 2D to 3D transformation algorithms.

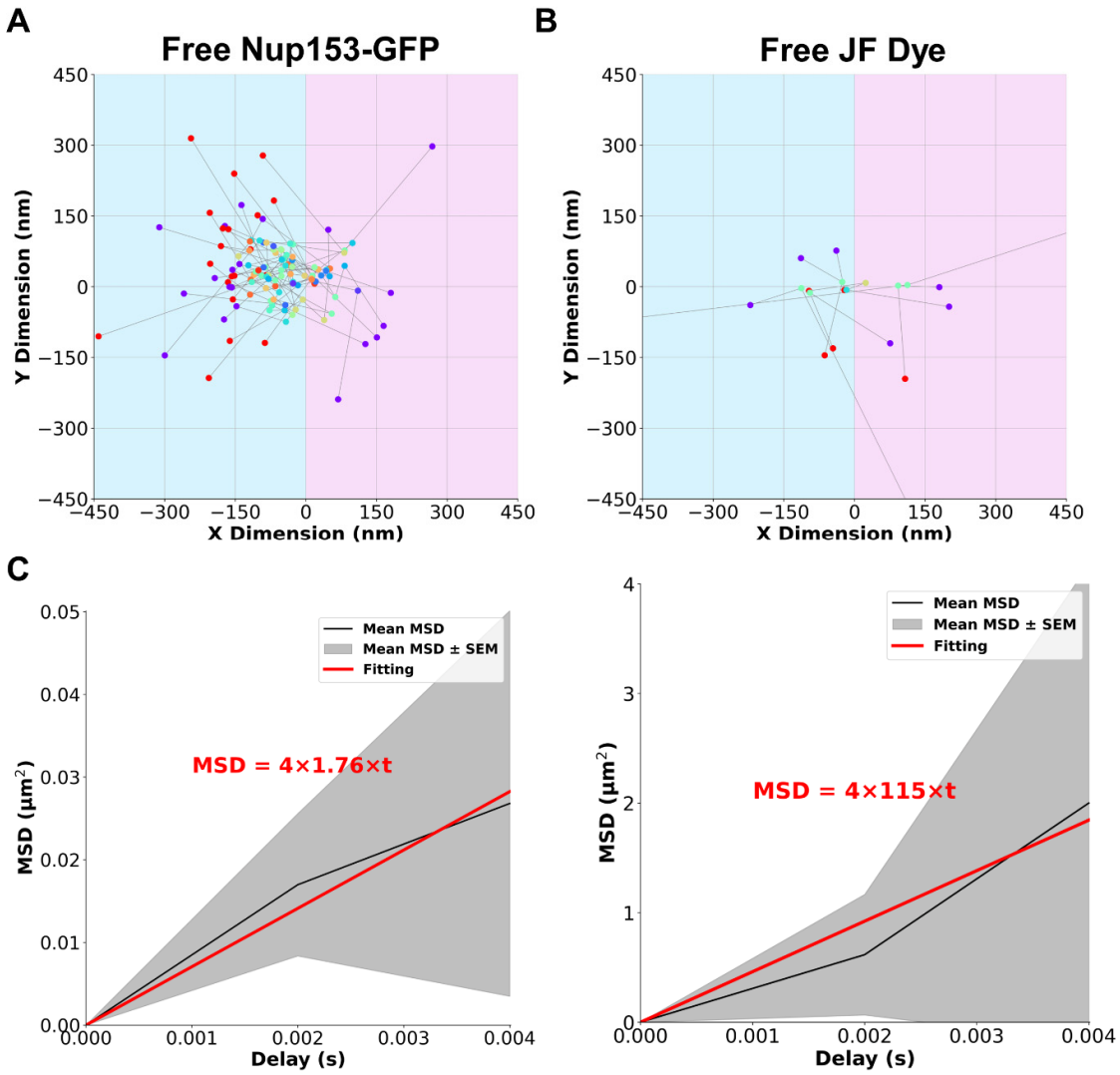

Figure S3. Passive diffusion of free JF dyes and unbound Nup153 observed at 2-ms capture rate

(A-B) These panels depict the trajectories of unbound Nup153-GFP and free JF 646 dye, observed at a 2 ms capture rate. The background is color-coded to indicate the localization relative to the NPC centroid, with blue representing the cytoplasmic region and pink representing the nucleoplasm. (C-D) In these panels, the mean MSD is represented in black, while the MSD ± SEM is shown in grey. A linear fitting is depicted in red. The red equation follows the relationship 4Dt, where "4" denotes that the diffusion is calculated using 2D information, D represents the diffusion coefficient, and t is the timeframe of capture.

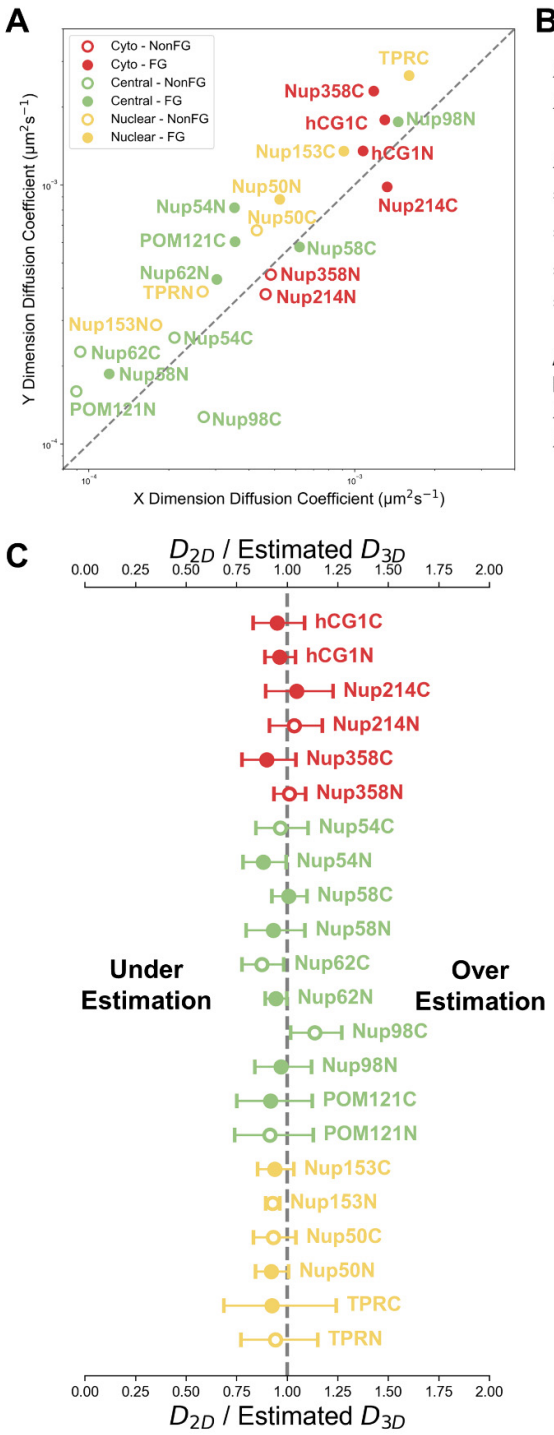

Figure S4. A comparison of the calculated 1D and 2D diffusion coefficients against an estimated 3D Diffusion Coefficients

(A) This panel presents a comparison between the X-dimension and Y-dimension diffusion coefficients. Both diffusion coefficients were calculated using the same trajectories and methodology as presented in Figure 2. A dotted line represents a reference line indicating a perfect 1:1 relationship between the X and Y dimensions.

(B) In this panel, the mathematical equations used to estimate the 3-dimensional diffusion coefficient from the X and Y dimensions are illustrated. (C) This panel displays the ratio of the calculated 2D diffusion coefficient over the estimated 3D diffusion coefficient. Error bars indicate a possible range for the ratio, derived from (2D diffusion coefficient + SE)/(3D diffusion coefficient - SE) and (2D diffusion coefficient - SE)/(3D diffusion coefficient + SE). A dashed vertical line represents a reference line indicating a ratio of 1. Plots to the left of this line suggest a possible underestimation of the diffusion coefficient.

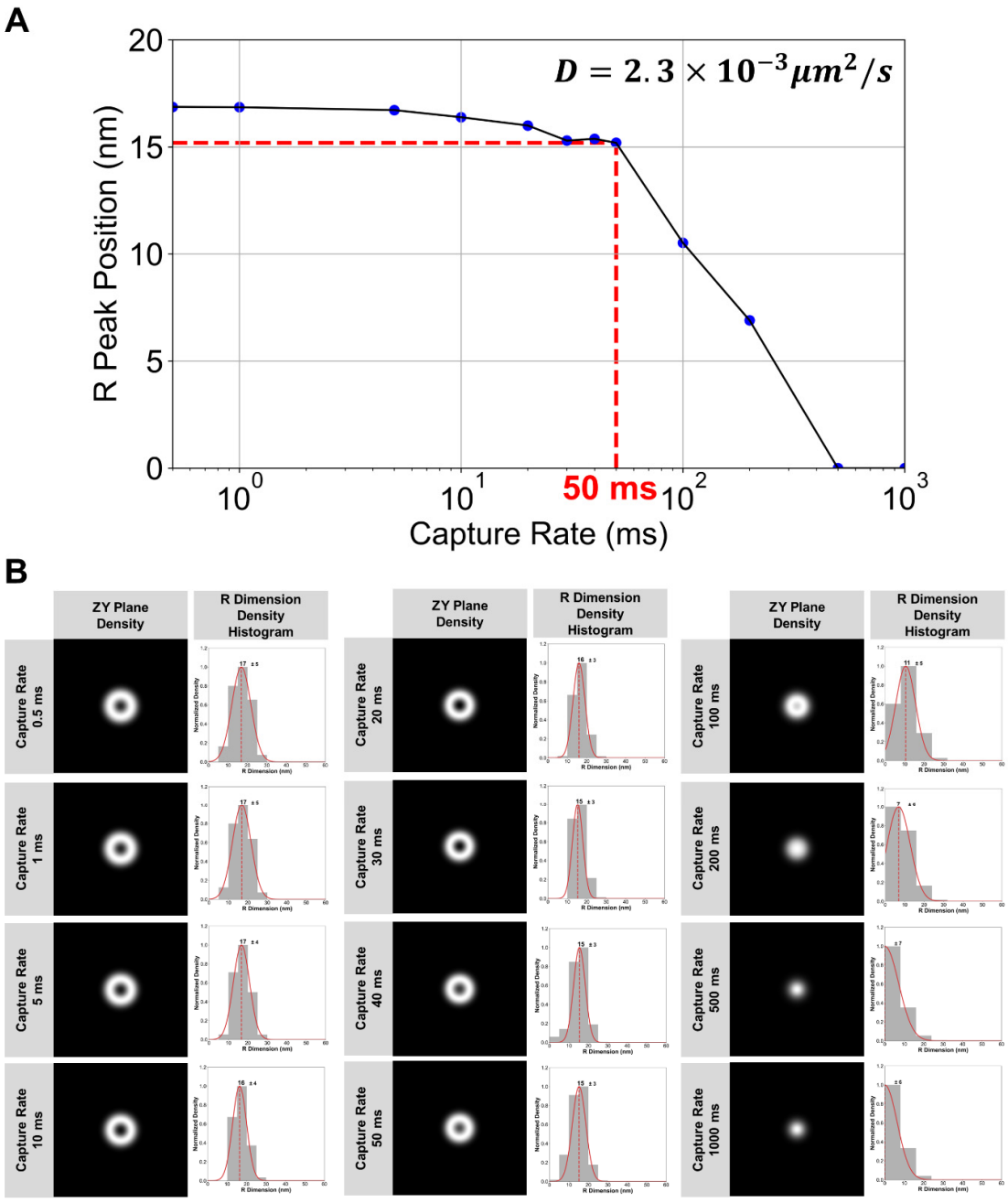

Figure S5. The effect of capture rate on 2D to 3D transformed R peak positions.

We conducted a Monte Carlo simulation [2,3] involving a ball-and-stick Nup analog within an NPC-like structure, utilizing a diffusion coefficient of 2.3x10^-3 μm^2/s. Single molecule localizations were collected at intervals of 0.5 ms, 1 ms, 5 ms, 10 ms, 20 ms, 30 ms, 40 ms, 50 ms, 100 ms, 200 ms, 500 ms, and 1000 ms. (A) Scatter Plot of Calculated R Peak Position vs. Capture Rate. This panel displays a scatter plot illustrating the calculated R peak position in relation to the capture rate. The 50 ms capture rate, which represents the conditions employed in this study, is highlighted with a red line. (B) 2D to 3D Transformed R-Dimension Density

Histograms and YZ Plane Density Ring. In this section, we present 2D to 3D transformed R-dimension density histograms and the generated YZ plane density ring at each capture rate.

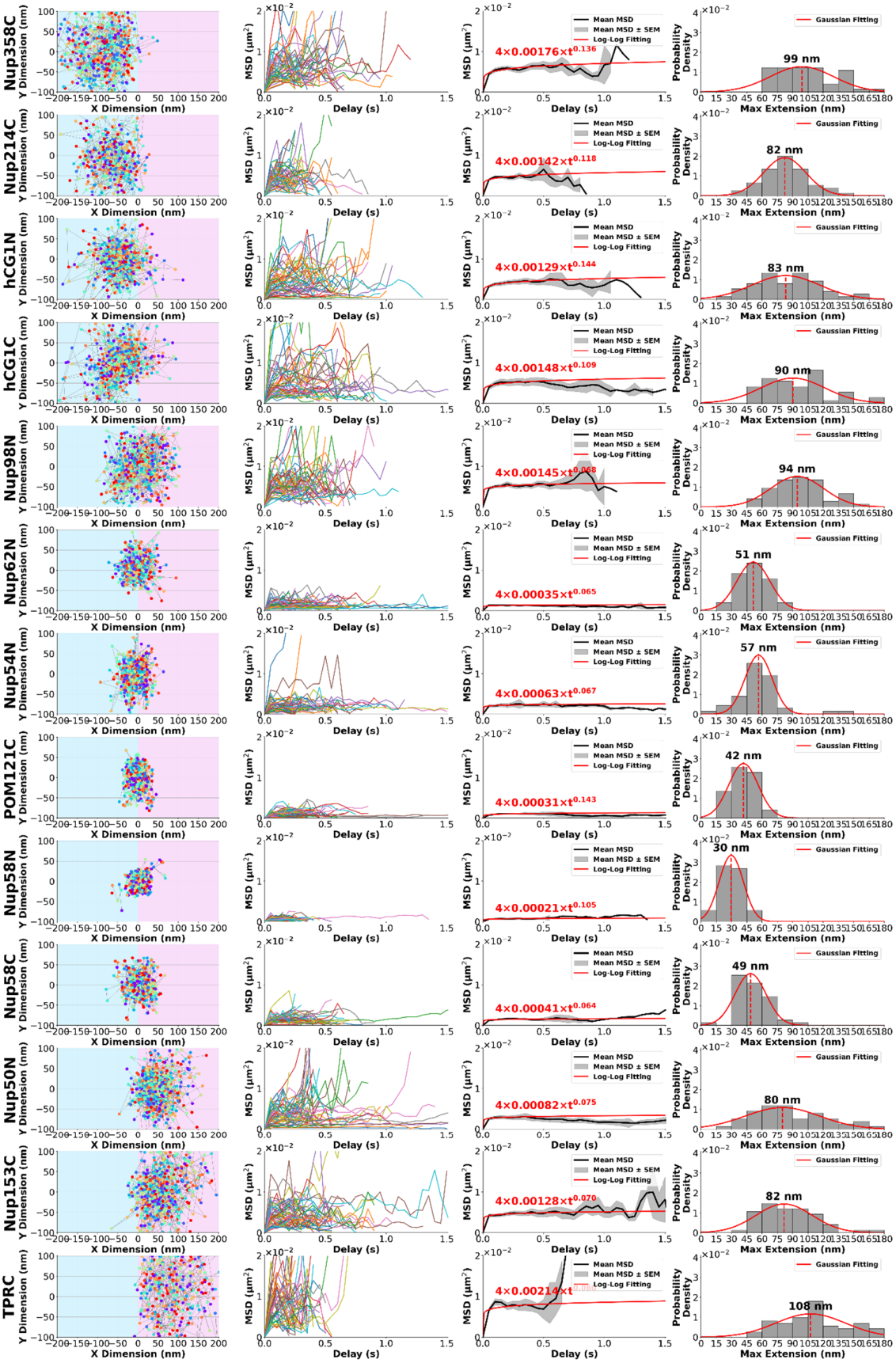
Nup358C
Nup214C
hCG1N
hCG1C
Nup98N
Nup62N
Nup54N
POM121C
Nup58N
Nup58C
Nup50N
Nup153C
TPRC
X Dimension (nm)
Y Dimension (nm)
MSD (μm²)
Delay (s)
Mean MSD
Mean MSD ± SEM
Log-Log Fitting
4×0.00176×t^0.136
4×0.00142×t^0.118
4×0.00129×t^0.144
4×0.00148×t^0.109
4×0.00145×t^0.088
4×0.00035×t^0.065
4×0.00063×t^0.067
4×0.00031×t^0.143
4×0.00021×t^0.105
4×0.00041×t^0.064
4×0.00082×t^0.075
4×0.00128×t^0.070
4×0.00214×t
Probability Density
Max Extension (nm)
Gaussian Fitting
99 nm
82 nm
83 nm
90 nm
94 nm
51 nm
57 nm
42 nm
30 nm
49 nm
80 nm
82 nm
108 nm

Figure S6. Live cell two-dimensional dynamics of FG-rich-terminal domains of FG Nups

In this figure, we present the FG-rich terminal domain for each FG Nup. The leftmost panel displays all traces, each consisting of a minimum of four consecutive frames for that specific domain. The background color distinguishes the localization relative to the NPC equator, with blue representing the cytoplasmic region and pink representing the nucleoplasm. The second panel from the left showcases the resulting Mean Squared Displacement (MSD) traces for the discrete traces in the first panel. Moving to the third panel, we illustrate the mean MSD (in black), the MSD ± SEM (in grey), and a log-log fitting curve (in red). The red equation follows the relationship $4Dt^{\alpha}$, where "4" denotes the calculation using 2D information, D represents the diffusion coefficient, t stands for the timeframe of capture, and α signifies the slope of the log-log fitting. In the fourth panel, we indicate the maximum extension of the recorded traces.

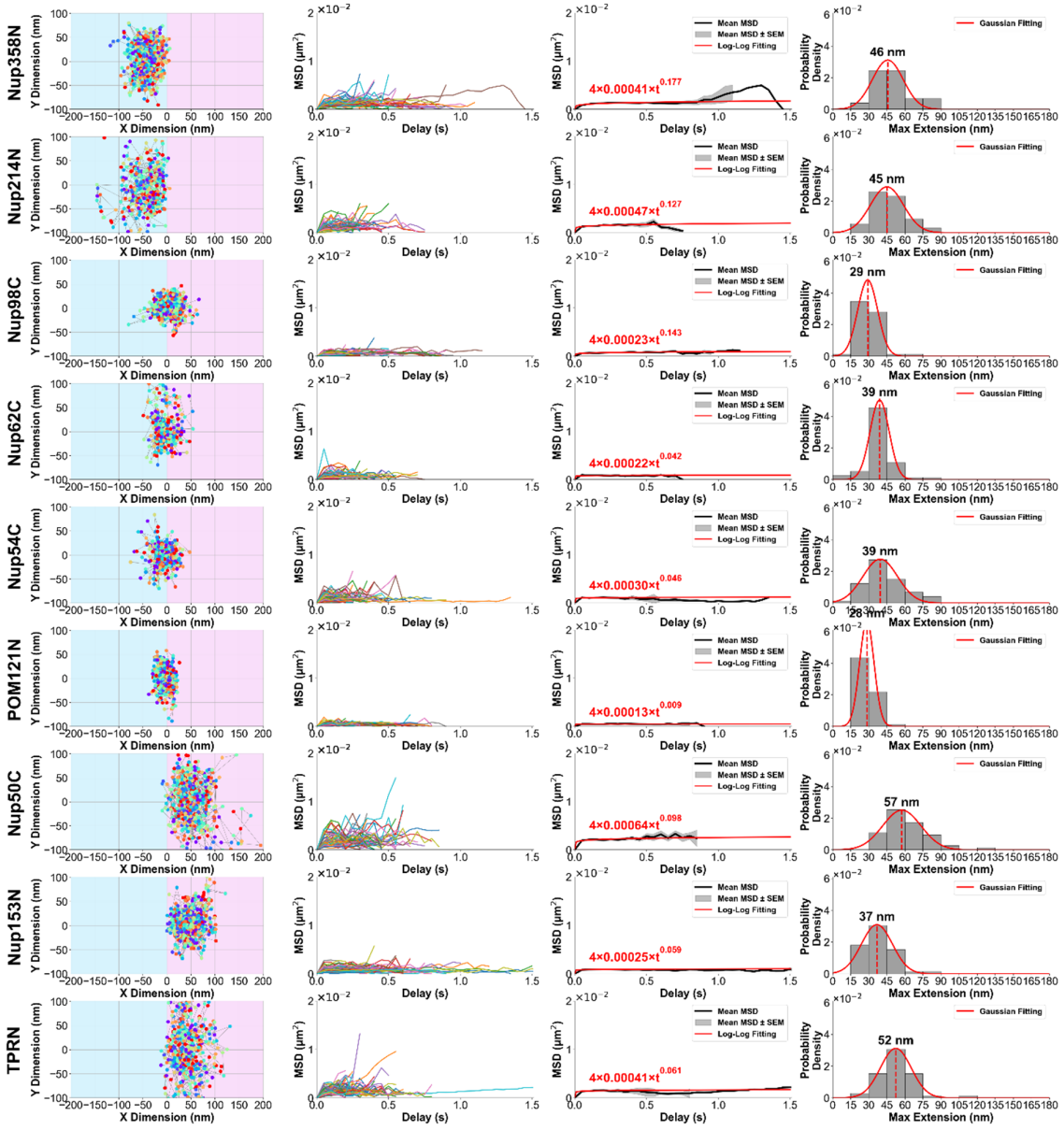

Figure S7. Live cell two-dimensional dynamics of non-FG-rich terminal domains of FG-Nups. In this figure, we present the non-FG rich terminal domain for each FG Nup. The leftmost panel displays all traces, each consisting of a minimum of four consecutive frames for that specific domain. The background color distinguishes the localization relative to the NPC equator, with blue representing the cytoplasmic region and pink representing the nucleoplasm. Moving to the second panel from the left, we showcase the resulting Mean Squared Displacement (MSD) traces for the discrete traces in the first panel. In the third panel, we illustrate the mean MSD (in black), the MSD ± SEM (in grey), and a log-log fitting curve (in red). The red equation follows the relationship 4Dt^α, where "four" denotes the calculation using 2D information, D represents the diffusion coefficient, t stands for the timeframe of capture, and α signifies the slope of the log-log fitting. Lastly, in the fourth panel, we indicate the maximum extension of the recorded traces.

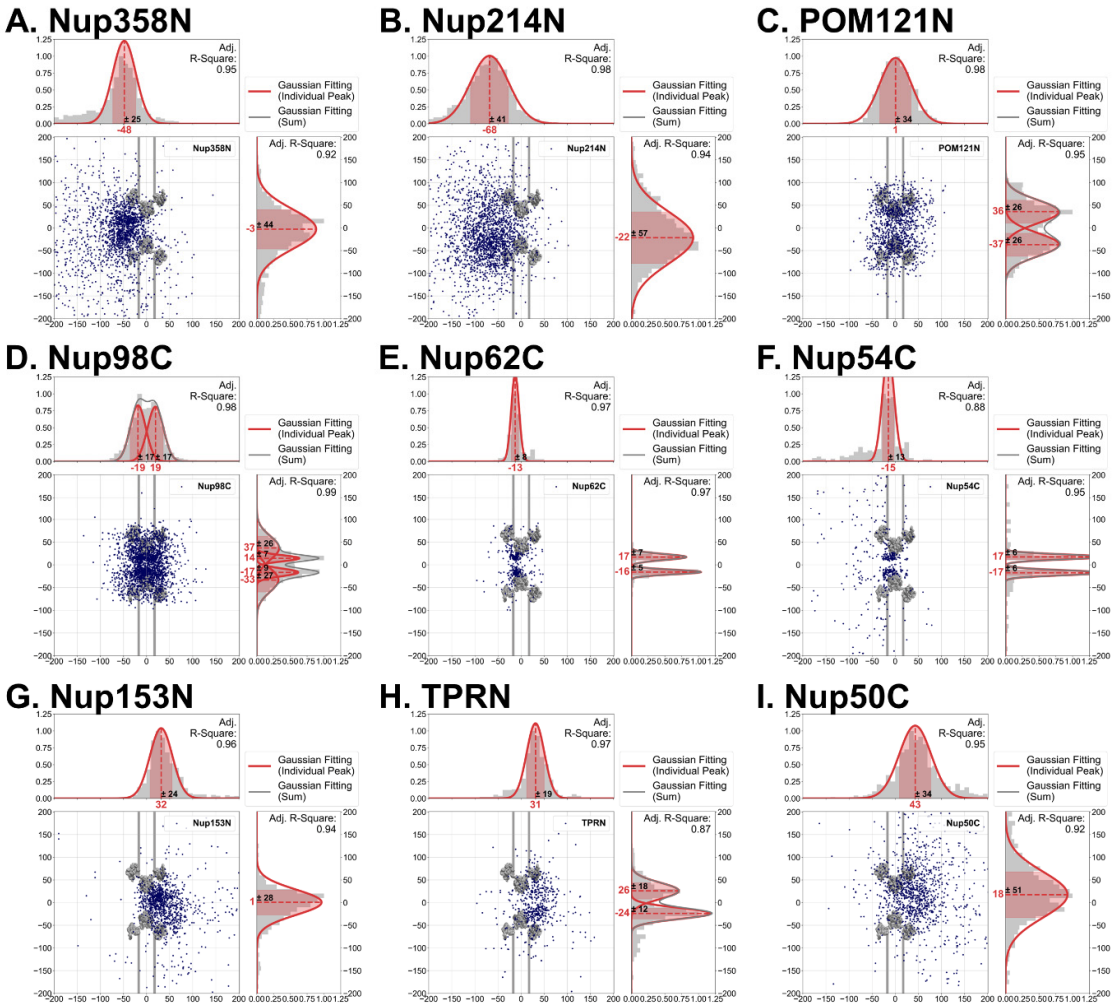

Figure S8. 2D spatial localizations for non-FG-rich Nup termini.

The 2D spatial localizations for the non-FG-rich termini were analyzed using density histograms fitted with a Gaussian function on the X and Y axes, respectively.

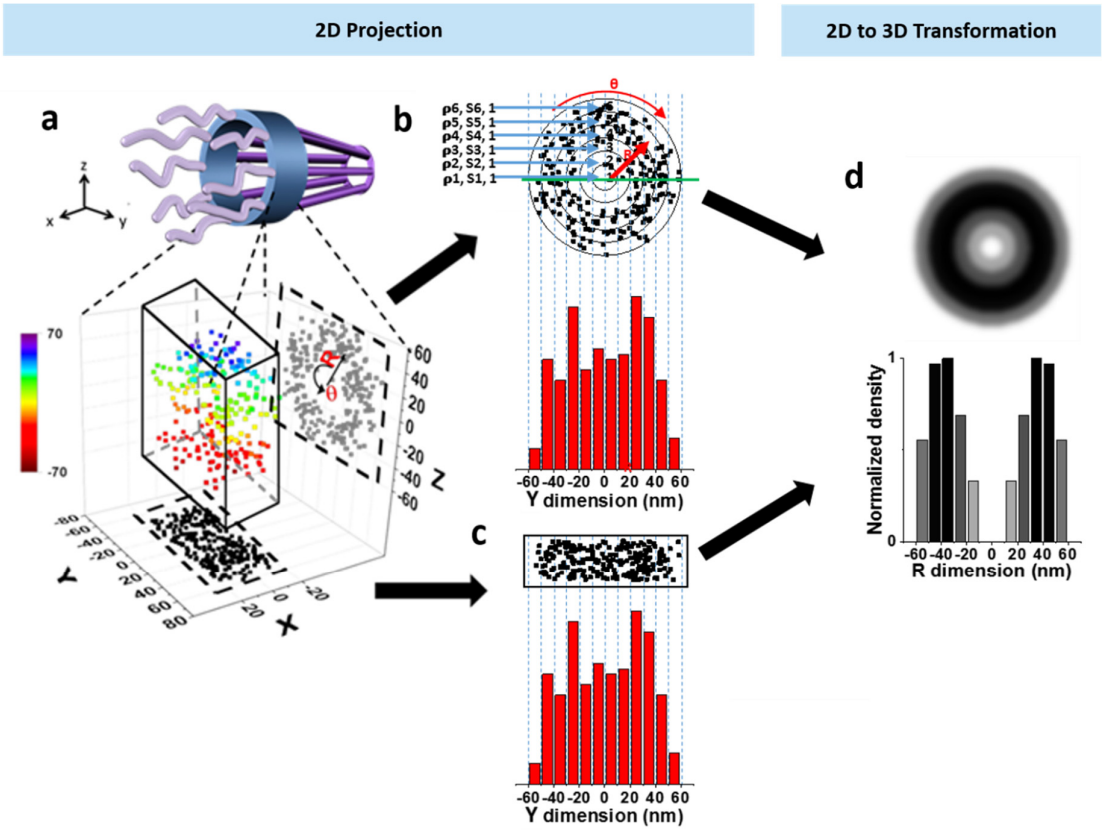

Figure S9. A schematic demonstration, with simulated data, of the 2D to 3D transformation algorithms for molecules that diffuse through the NPC. (A) 3D spatial locations of randomly diffusing molecules inside the NPC can be coordinated in a cylindrical coordination system (R, Θ, Y) due to the cylindrical rotational symmetry of the NPC. The 3D molecular locations in the NPC (rainbow colored for Z position) are projected onto a 2D plane in a Cartesian coordination system (X and Y, shown as black points) by microscopy imaging (Y and Z, shown as gray points). (B) The cross-sectional view of all the locations is shown in Figure S5A (same as the gray points from the Y and Z dimension). These locations can be grouped into sub-regions between concentric rings. Given the high number of randomly distributed molecules in the NPC, the spatial density of locations ($\boldsymbol{\rho i}$) in each sub-region ($\boldsymbol{s(i,j)}$) between two neighboring rings will be rotationally symmetrical and uniform. These locations can be further projected into 1D along the Y dimension. The locations along the Y dimension can be clustered in a histogram with j columns. The total number of locations in each column ($\boldsymbol{A(i,j)}$) is equal to $2 \times \sum_{i=j}^{n} \rho_i \times s_{(i,j)}$, which is further explained in Figure S5. (C) Histograms of 2D projected data from microscopy experiments are identical to B, thereby allowing us to use the aforementioned formula to determine the density of each concentric ring. D). Using the algorithms, 2D projected data can be used to reconstruct the 3D spatial distribution of protein location on the NPC. The figure was reproduced from our previous publication with permission.[5-9]

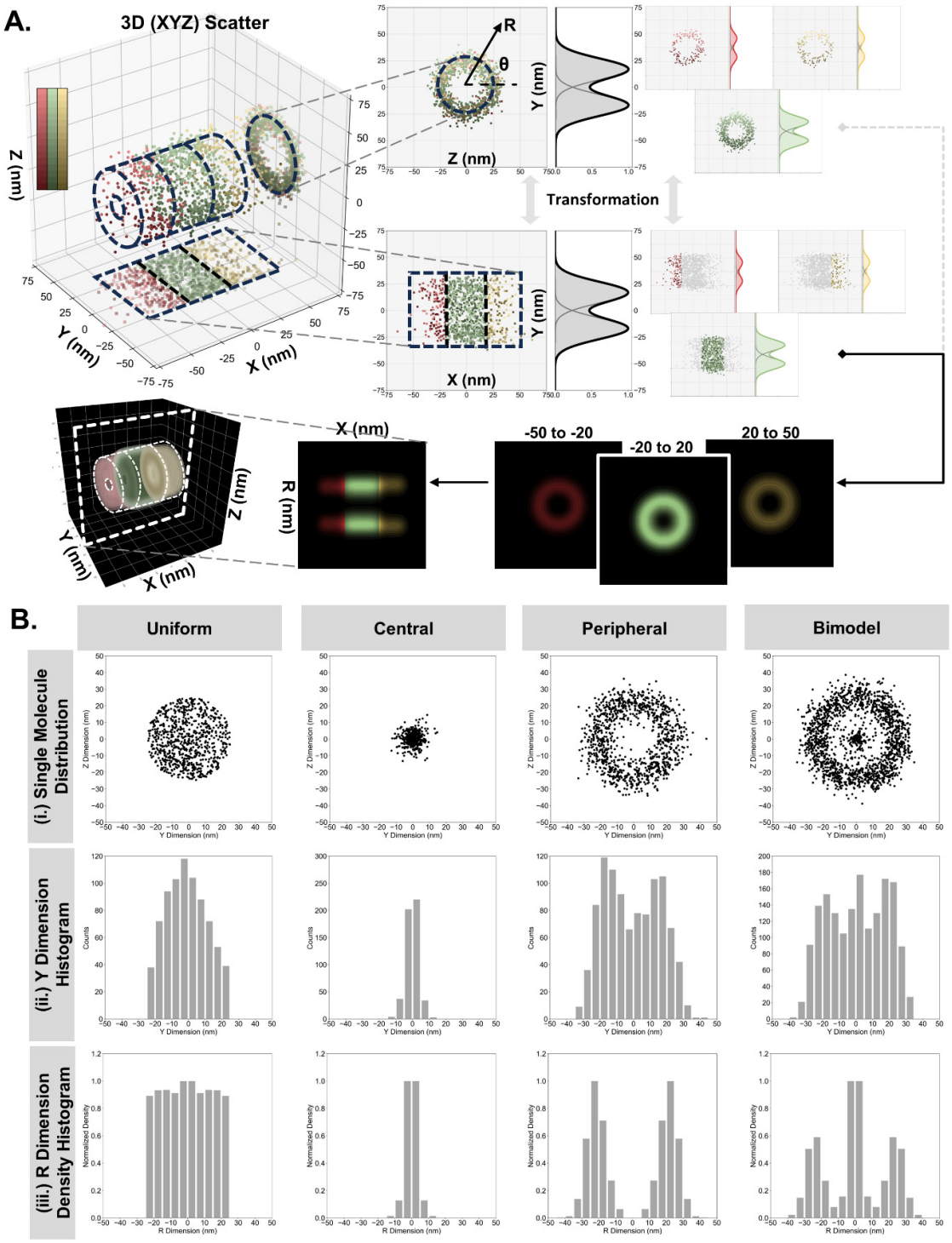

Figure S10. 2D to 3D transformation and Simulated localization distribution for existing NPC models.

(A) Schematic Representation of 2D to 3D Transformation Algorithms. In this panel, we provide a schematic demonstration using simulated data to illustrate the 2D to 3D transformation algorithms applied to molecules within the NPC. The plotted three-dimensional data are generated along rotationally symmetrical localizations, which

can be projected onto both the XY and YZ planes. Localizations are categorized into different regions based on their X-dimension positions, labeled with distinct colors. Similar to the data obtained from microscopic imaging, the XY projections are transformed into vertical 3D maps for individual regions. These 3D maps for all regions are then combined to produce the final comprehensive 3D map. (B) Simulated YZ Dimension Localization Distributions. In this section, we present simulated YZ dimension localization distributions for various models representing the transit of single molecules through the central channel of the NPC. (B_i) Sample Data Sets. Subpanel (B_i) displays sample data sets derived from simulation runs, illustrating the uniform, peripheral, central, double peripheral, and bimodal distributions, respectively. (B_{ii}) Y-Dimensional Histograms. Subpanel (B_{ii}) presents Y-dimensional histograms corresponding to the data sets shown in (B_i). (B_{iii}) 3D Density Histograms. Finally, in subpanel (B_{iii}), we showcase 3D density histograms that are calculated based on the information presented in panels (B_i) and (B_{ii}).

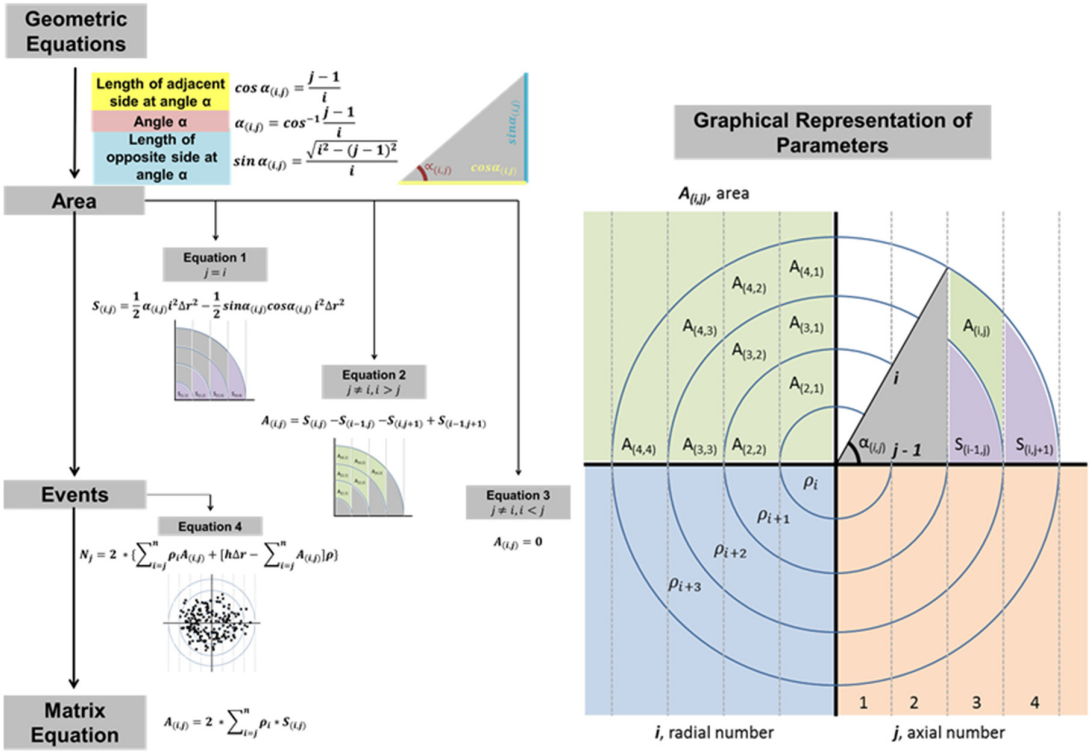

Figure S11.Matrix equation flowchart.

($\boldsymbol{A_{(i,j)}}$), area of the sub-region, (i), radial number, (j), axial number, ($\boldsymbol{\rho_i}$), spatial probability density in each radial ring, ($\boldsymbol{S_{(i,j)}}$), area of the sub-region, ($\boldsymbol{N_j}$), number of events, and ($\Delta \boldsymbol{r}$), bin size. Equations 1 – 3 will determine the area of the sub-region given certain parameters (i.e., i = j). Equation 4 will determine the number of events in the given area. Once the subregion area ($\boldsymbol{A_{(i,j)}}$) and events ($\boldsymbol{N_j}$) are known, the spatial probability density in each radial ring ($\boldsymbol{\rho_i}$) can be calculated.

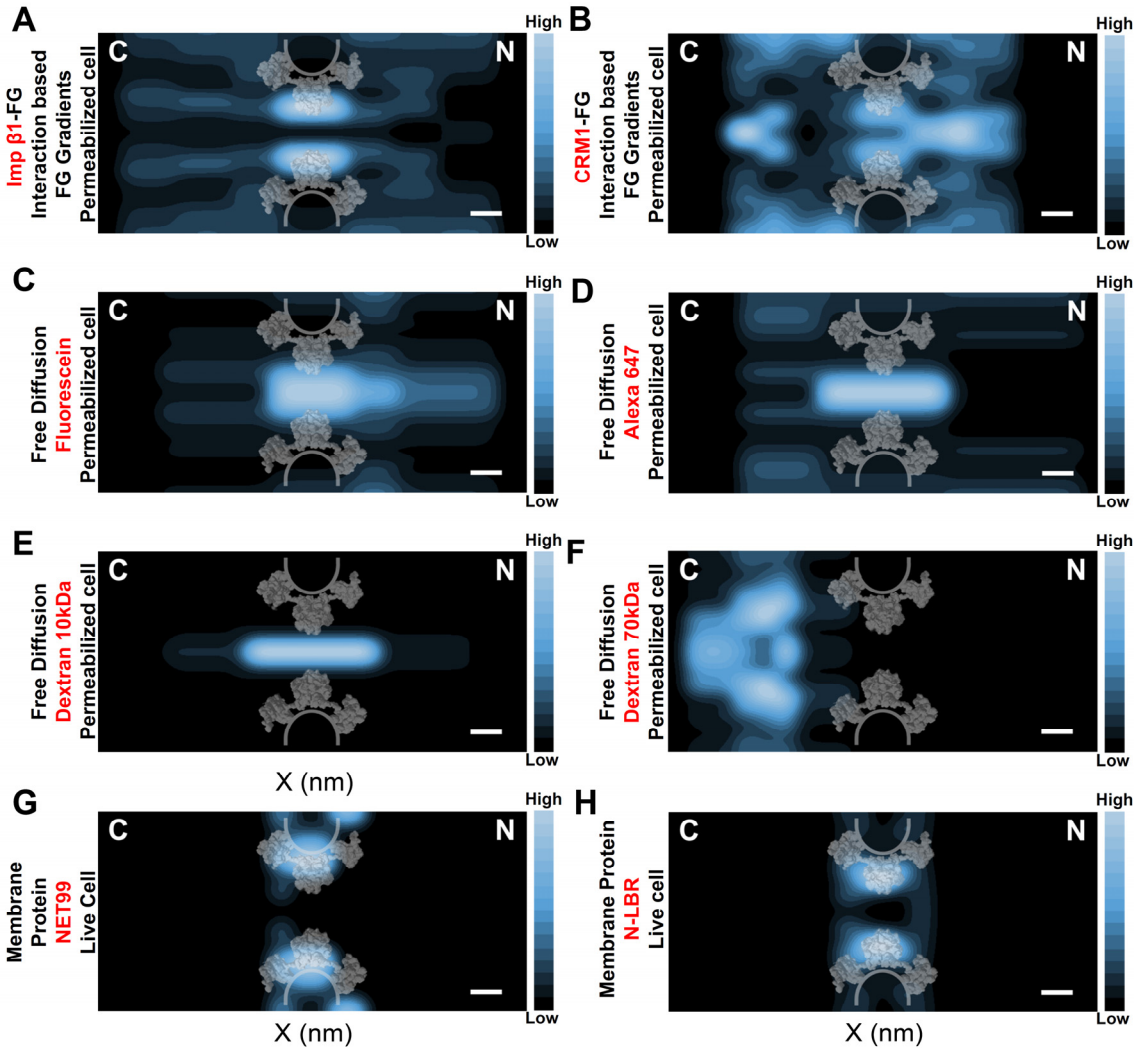

Figure S12. 3D probability density maps of various transiting macromolecules in live and permeabilized cells.

(A) 3D Probability Density for Importin-β1 Transit[4]. Panel (A) displays the 3D probability density map for the transit of Importin-β1 through the NPC in permeabilized cells. (B) 3D Probability Density for CRM1 Transit[4]. Similarly, in panel (B), we depict the 3D probability density map for the transit of CRM1 through the NPC in permeabilized cells. (C-D) 3D Probability Density for Passive Diffusion of Molecules[5]. Panels (C-F) show the 3D probability density maps for the passive diffusion of molecules ranging in size from 0.3 kDa to 70 kDa. (G-H) 3D Probability Density for Transmembrane Proteins Transit[6]. In these panels, (G-H), we present the 3D probability density maps for the transit of transmembrane proteins, N-LBR, through the NPC. Data was collected from our previous publications and reanalysised with methodologies used in this study for consistency. Scale bar: 20 nm. N: nucleus. C: cytoplasm. Data for panels A-B are reproduced here with permission from Nature Publishing[4]. Data for panels C-F are reproduced with permission from

the Proceedings of the National Academy of Science[5]. Data for panels G-H are reproduced with permission from Nature Publishing[6].

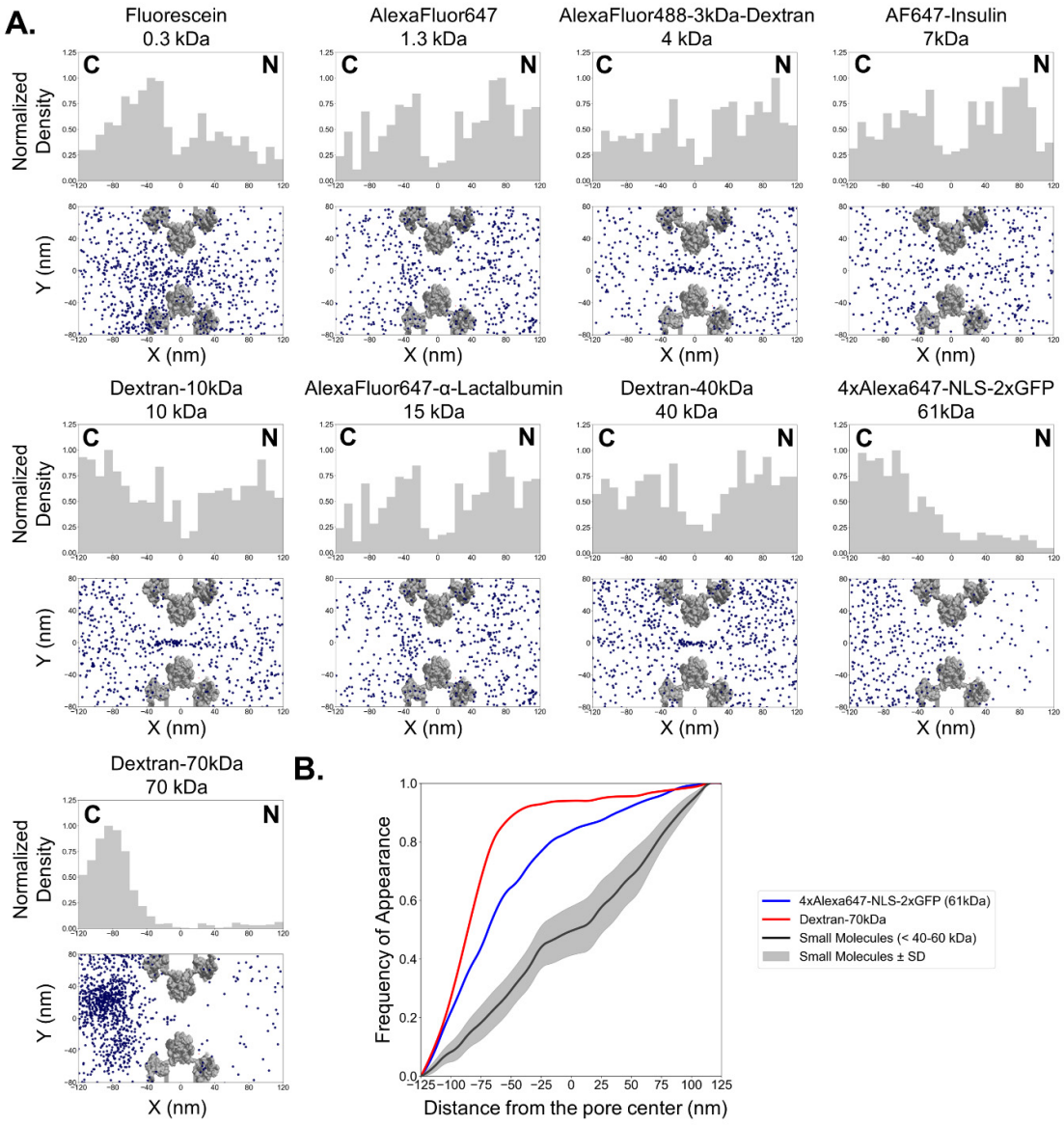

Figure S13. Frequency of Occurrence for Passive Diffusion Molecules at Varying Distances from the Pore Center

(A) 2D Localizations of Passively Diffusing Molecules. We present 2D localizations of passively diffusing molecules of various sizes, depicted as scatter plots with density histograms along the x-dimension. (B) Cumulative Frequency vs. Distance from Pore Center. Panel (B) displays the cumulative frequency of appearance for each molecule plotted against their respective distance from the pore center. The black line, accompanied by a grey area, represents the mean ± standard deviation (SD) for small molecules with molecular weights ranging from below 40 to 60 kDa.

Additionally, blue and red lines represent passively diffusing molecules exceeding the diffusion limits, specifically at 61 kDa and 70 kDa, respectively.

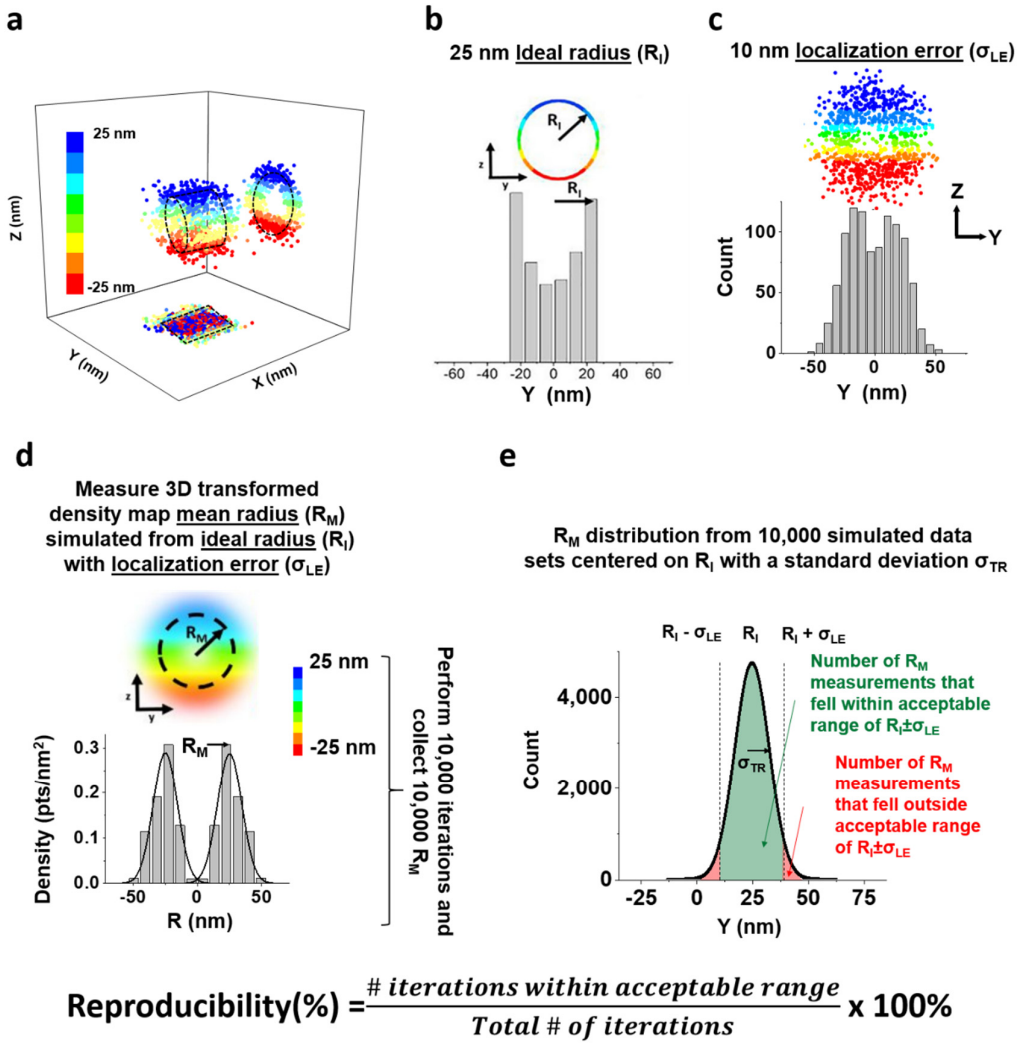

$$\text{Reproducibility(\%)} = \frac{\#\ iterations\ within\ acceptable\ range}{Total\ \#\ of\ iterations} \times 100\%$$

Figure S14. Calculating reproducibility percentage

For any given set of simulated data, the bin size was varied from 1 nm to the precision, which is 10 nm in this example, and the optimal bin size was selected according to a Chi-square analysis from our previous publication. For actual calculations, the associated mean precision was used for each FG-Nup. **(A)** Data sets were simulated in three dimensions. The color bar indicates the Z position of the simulated points. **(B)** Each data set was simulated first with an ideal radius (R_I), which was 25 nm in this example. This represents the diameters allowed within the central channel of the NPC. Radi between 25-110 nm was used for sub-regions within the cytoplasmic side. For nuclear basket sub-regions, radii of 25-100 were utilized to account for the more considerable freedom of movement allowed in those sub-regions **(C)** Subsequently, a localization error (σ_{LE}), 10 nm in this example, was added to each point. Using a 5-nm optimal bin size for demonstration, the 2D histogram of the simulated data set with a 25-nm radius and 10-nm localization

precision was determined. **(D)** One thousand data sets were simulated with an ideal 25-nm radius (R_I) and a localization error (σ_{LE}) of 10 nm. The resultant 3D histograms were then each fitted with a Gaussian function to localize the mean position of each peak, which is designated as the mean radius (R_M). **(E)** The histogram for all the R_M values was determined, and two parameters were obtained: the reproducibility percentage and the standard deviation of the R_M peak fittings. **(F)** For the reproducibility percentage, the number of simulated data sets that fell within the acceptable range of $R_I \pm \sigma_{LE}$ were counted. The acceptable range of $R_I \pm \sigma_{LE}$ was chosen because, in principle, the resolution of any two Gaussian fittings is limited to the standard deviation or spread of those peaks, which is due to the simulated localization error (σ_{LE}) in our simulation and contributed to by the single molecule localization error in our experiments. For the standard deviation of the peak fits, the term describes how wide the R_M peak fits were distributed and is designated as σ_{TR}. After 1,000 simulations, the histogram for R_M values converges on the mean (R_I) from which they were originally sampled, while the spread of the R_M histogram (σ_{TR}) converges on a value that is due to the number of simulated points in each distribution and simulated localization error.

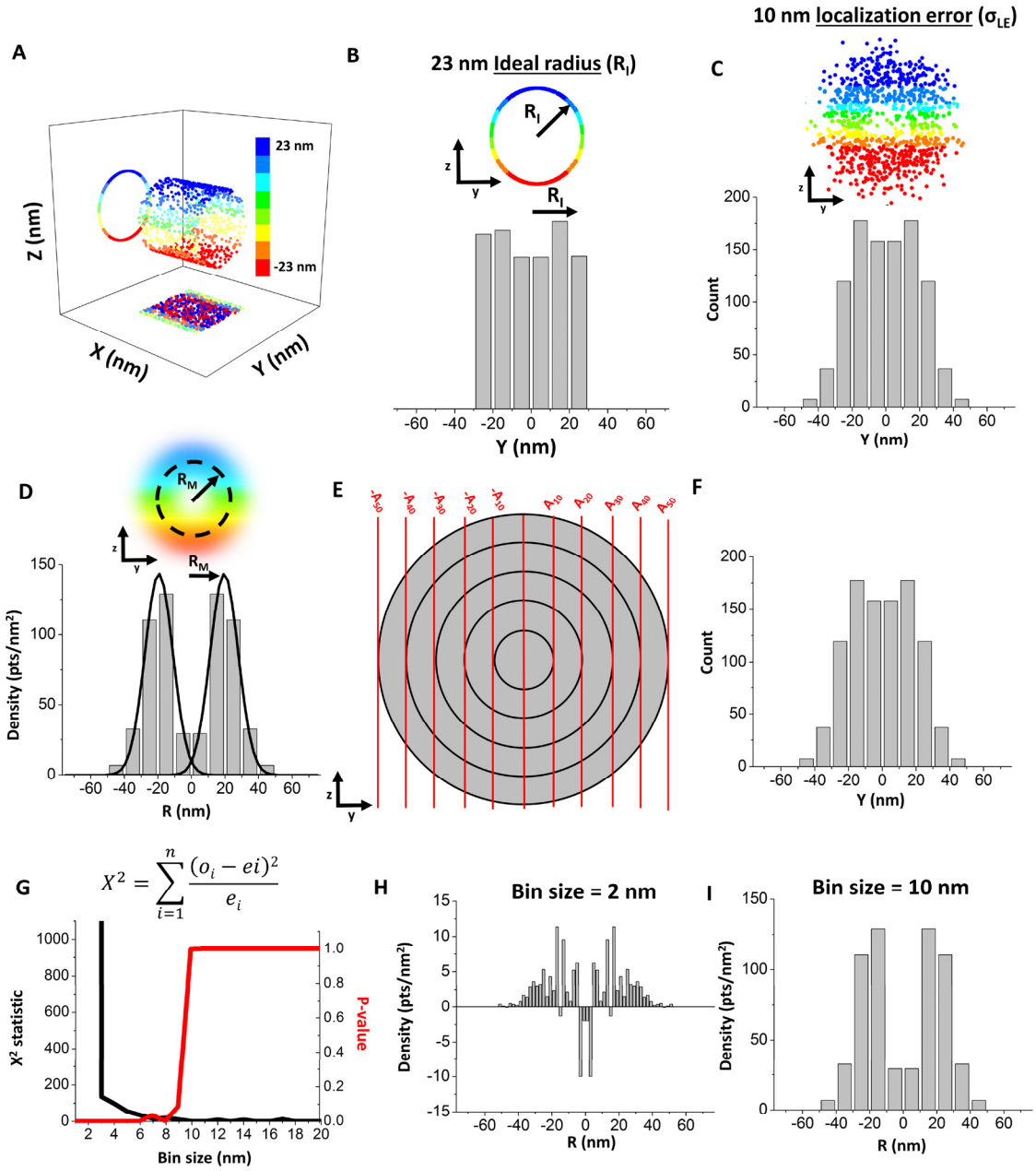

Figure S15. Optimal bin-size determination using Chi-square error and P-value analysis.

For any given set of simulated data, the bin size is varied from 1 nm to the precision that is 10 nm in this example. **(A)** Data sets were simulated in three dimensions. The color bar indicates the z position of the simulated points. This representative data set contains 1,000 single molecule locations. **(B)** Each data set was simulated first with an ideal 23-nm radius (RI). **(C.** Subsequently, a localization error (σ_{LE}) of 10 nm was added to each point. Using a 10-nm bin size for demonstration, the 2D histogram of the simulated data set with a 23-nm radius and 10-nm localization precision was determined. **(D)** The 3D density histogram was then obtained via the 2D to 3D

transformation algorithm and the peaks were fit with Gaussian distributions. **(E).** The 10-nm bin-size area matrix was calculated and multiplied by the 3D density distribution in (D) to reconstruct the 2D distribution (any negative values in the density distribution were set to zero) as shown in F. **(F)** The values of the reconstructed 2D distribution were then compared bin-by-bin to the original 2D distribution (as shown in C) using the Chi-square analysis equation where 'o' refers to the observed histogram values in (F), 'e' refers to the expected histogram values in (C), 'i' refers to the bin, and 'n' refers to the total number of bins with histogram values in them. **(G)** The Chi-square test statistic and p-value were then plotted across the potential bin size values. A p-value ≤ 0.01 indicates that the 2D histograms in (C) and (F) are different from each other, suggesting the lack of enough data to allow sufficient sampling from each bin. On the other hand, a p-value > 0.99 suggests that the 2D histograms are statistically similar and likely have enough data points to accurately measure the value in each bin. Chi-square analysis was performed 1,000 times for each set of simulation parameters. **(H)** A 3D density histogram displaying large errors (negative density values) due to a bin size selection that was too small. Such errors occur when the single molecule density is not uniform throughout a given radial bin. This non-uniformity is due to under-sampling. **(I)** A 3D density histogram displaying no errors and a clear Gaussian distribution due to a properly selected bin size. A larger bin size can smooth the effects of under-sampling to a certain degree.

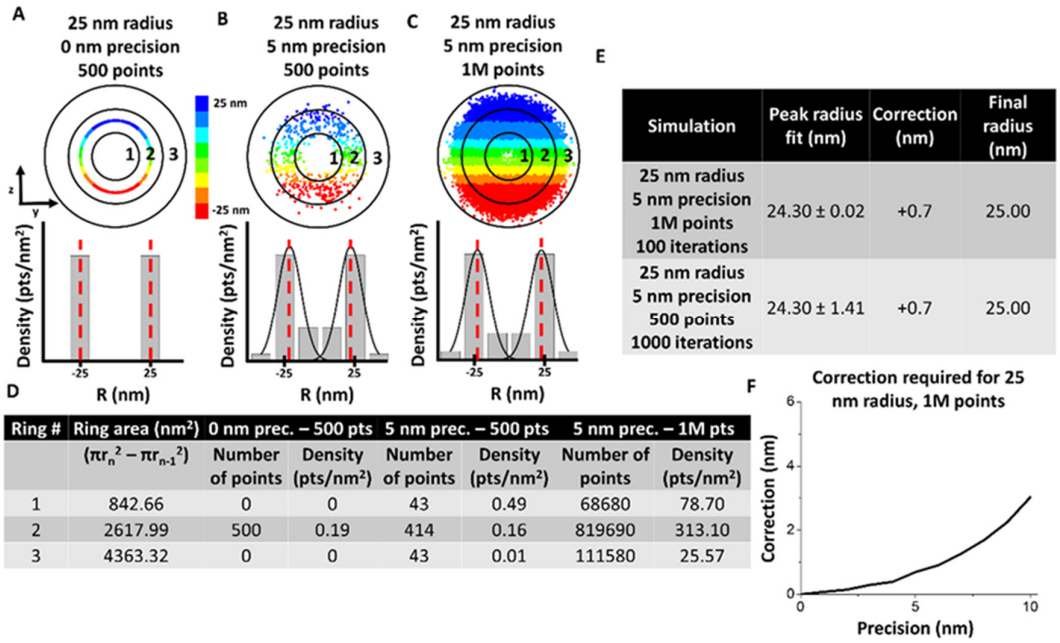

E

Simulation	Peak radius fit (nm)	Correction (nm)	Final radius (nm)
25 nm radius 5 nm precision 1M points 100 iterations	24.30 ± 0.02	+0.7	25.00
25 nm radius 5 nm precision 500 points 1000 iterations	24.30 ± 1.41	+0.7	25.00

D

Ring #	Ring area (nm²)	0 nm prec. – 500 pts		5 nm prec. – 500 pts		5 nm prec. – 1M pts	
	$(\pi r_n^2 - \pi r_{n-1}^2)$	Number of points	Density (pts/nm²)	Number of points	Density (pts/nm²)	Number of points	Density (pts/nm²)
1	842.66	0	0	43	0.49	68680	78.70
2	2617.99	500	0.19	414	0.16	819690	313.10
3	4363.32	0	0	43	0.01	111580	25.57

Figure S16. Sensitivity of inner bins necessitates slight correction of peak position during simulation

A), **B)**, and **C)** showing simulated single molecule data and corresponding 3D density histograms. **A** is for simulation with a 25 nm radius, 0 nm localization error, and 500 points. Red dashed lines indicate mean peak fitting. **B**). Simulated single molecule data and corresponding 3D density histogram for simulation with 25 nm radius, 5 nm localization error, and 500 points. Red dashed lines indicate mean peak fitting. **C).** Simulated single molecule data and corresponding 3D density histogram for simulation with 25 nm radius, 5 nm localization error, and 1 million points. Red dashed lines indicate mean peak fitting. **D).** Table showing the calculation to obtain each bin of the 3D density histogram. **E).** Table showing that even one million points does reconstruct a precise 25 nm peak fitting due to the fact that the inner radial bins have smaller area and are slightly more sensitive to changes in density. **F).** Correction required for each precision up to 10 nm for a 25 nm radius. This correction process was performed before each simulation to accurately localize the R_M density peak and correlate it to the ideal R_I from which the data was simulated.

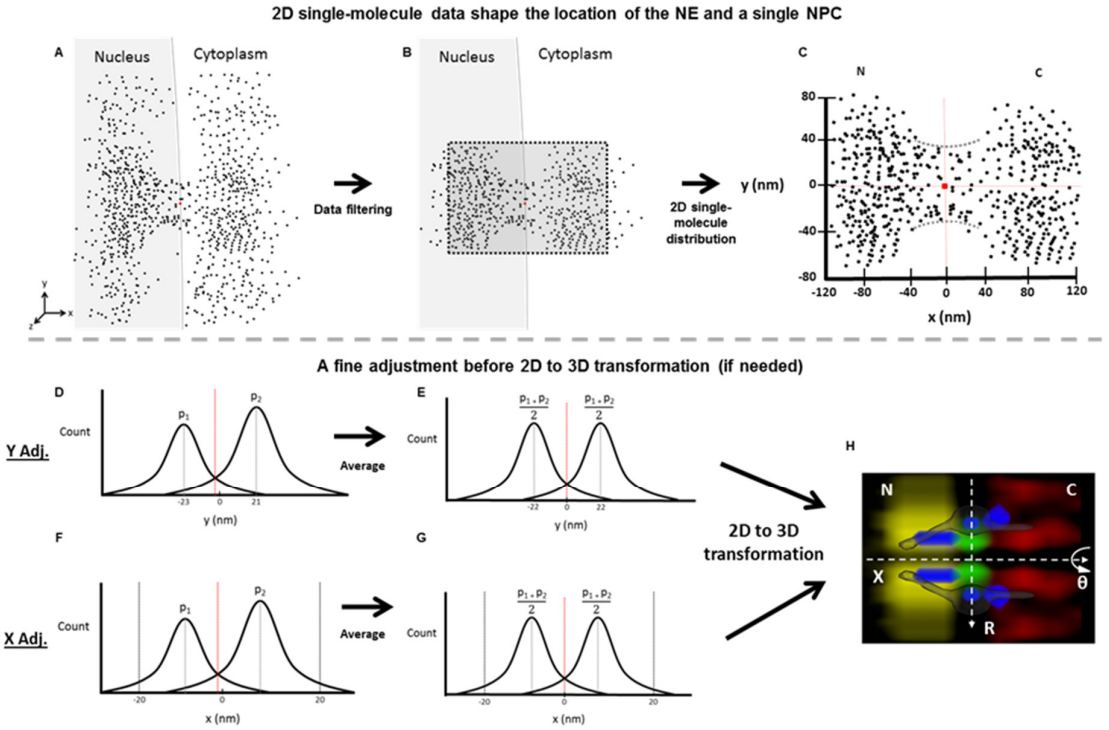

Figure S17. Determination of the central axis of the NPC illuminated by SPEED microscopy.

Diagrams are used to demonstrate the detailed steps in our data analyses. **A).** The initial single-molecule tracking data (black points) are plotted around the NPC's marker (red dot) collected with SPEED. **B).** The collected data after filtering by using single-molecule spatial localization precision. **C).** The filtered 2D single-molecule data shape the spatial location of the NE and a single NPC. The red dot represents the location of the NPC's marker. But sometimes, the marker's position is not perfectly overlapped with the averaged central positions in either x or y dimension suggested by the 2D single-molecule data. Also, the 2D single-molecule distribution also indicates the orientation of NPC. If the orientation of the NPC is within a free angle of 1.4° to the perpendicular direction to the NE, the 2D single-molecule data will be proceeded further. If the point is outside of the selected region, then point will be dropped. **D).** The plot of projected locations of these 2D single-molecule data in the y dimension will indicate if a fine adjustment for the central cytoplasmic transport axis is needed or not. Here we just show an example that peak 1 (p1) and peak 2 (p2) are not symmetrical locating at -23 nm and 21 nm respectively. If the peaks are symmetrical, the step E will be skipped to move onto the 2D to 3D transformation directly. **E).** The two peaks are averaged as ((p1 + p2)/2), resulting a fine adjustment in the NPC's central cytoplasmic transport axis. The dotted red line has shifted to the corrected central position. **F-G).** Similar to the y-dimensional data process, we next determine the precise location of the NPC's central position along the x dimension by fitting the histogram of these 2D single-molecule locations within the NPC's scaffold

region projected into the x dimension (ranging from -20nm to 20nm, as clearly shown in the void region of the NE in (C) even if the NPC's marker is a slightly off center). **H).** The 2D single-molecule data with the confirmed x and y axes will undergo the 2D to 3D transformation (Fig. S4) to produce the 3D density map of Nup153, POM121, and Nup214 FG-regions (yellow, green, and red clouds, repetitively) and anchoring regions (blue clouds). Figure reprinted with permission from the Proceedings of the National Acadamy of Sciences [7].

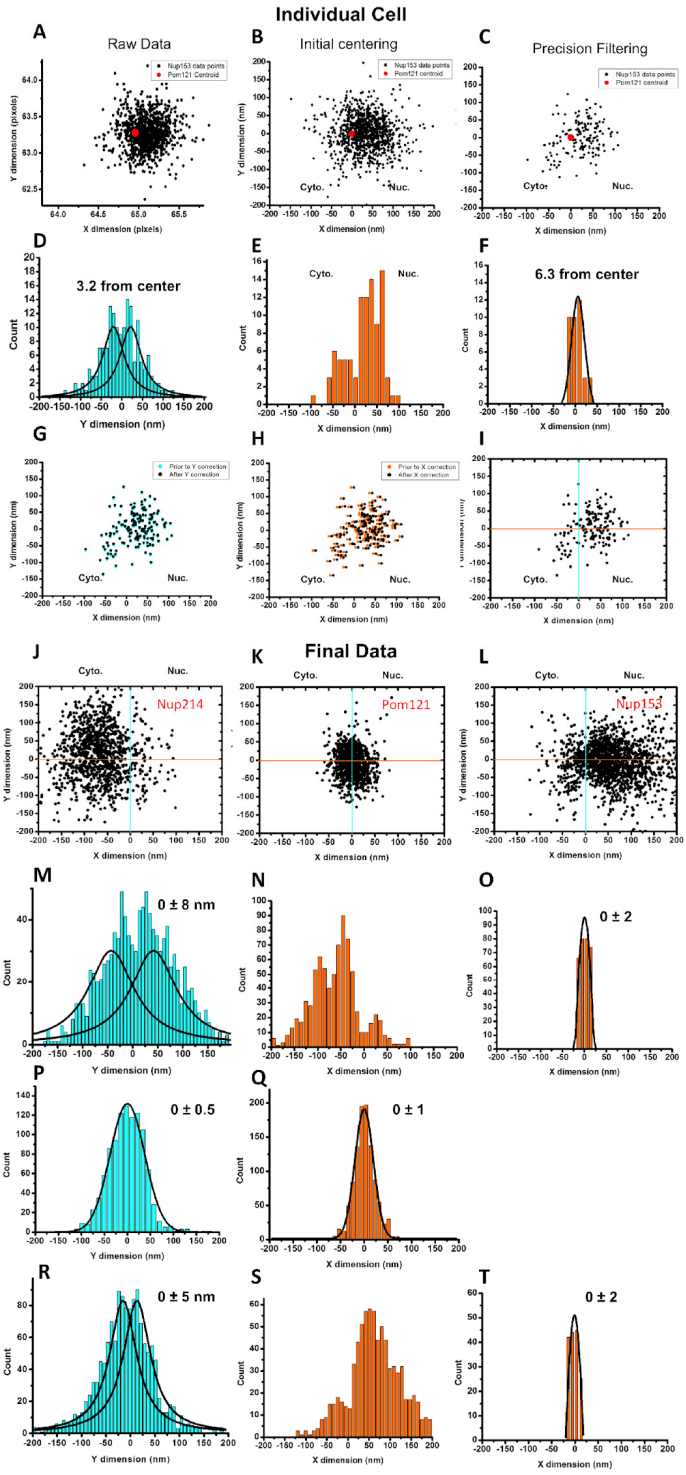

Figure S18. Overlapping 2D spatial data with the NPCs centroid

To correct experimental drifting errors, we applied a meticulous histogram analysis approach to center the spatial data collected for each FG-Nup. Using representative examples from different subregions of NPCs, namely Nup153 on the nuclear side,

POM121 at the central scaffold, and Nup214 at the cytoplasmic side, we demonstrated our method. (A) Initial raw data from a single-molecule video of Nup153 was gathered, where black dots represented the JF646 signal indicating the Nup153 C-terminal domain, and the red dot at the center indicated the centroid obtained from the POM121-mCherry signal. (B) The raw data was centered based on the acquired POM121 centroid, set as the reference at the 0, 0 position, and flipped for consistency across data. (C) Subsequently, the Nup153 data was filtered based on precision. (D) The Y-dimensional data was fitted to a symmetrical Gaussian function, recalibrating the data using obtained peak positions as shown in G. (E) X-dimensional histograms were used to further center the data in the X dimension. The region lacking data points, corresponding to the nuclear envelope region of the NPC, was fitted based on inversion and Gaussian fitting, leading to the re-centering shown in H. The final centered data is presented in I. The subsequent steps outlined the process of quantifying the final centroid error for each FG-Nup distribution. (J-L) Displayed the final data points acquired from multiple cells for Nup214, POM121, and Nup153, respectively. (M-T) Gaussian fitting errors in the Y and X dimensions of the histograms were utilized to calculate the ultimate centroid error. Notably, POM121, located at the centroid of the NPC, did not require inversion in the X dimension due to its higher density of points, corresponding to the nuclear envelope. The resulting final errors are detailed in Supplemental Table S2.

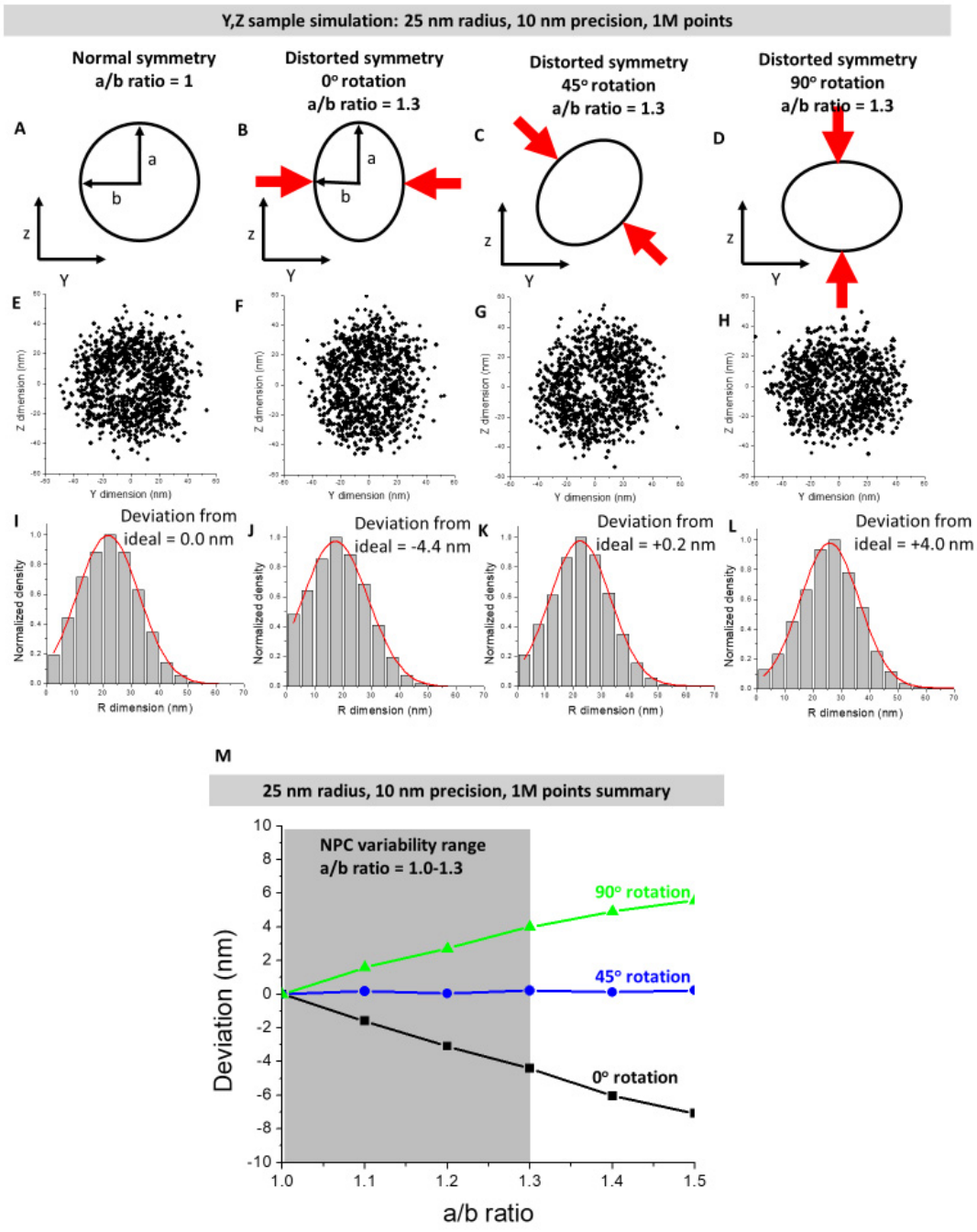

Figure S19. Varying the compression and rotation of the radial symmetry shows minimal effects under biological conditions.

(A) Ideally, the radial symmetry is perfect with both the a and b axes being equal in the y and z dimensions. (B–D) In some cases, compression may occur where the a and b axes are unequal and rotated at any angle relative to the compression axis. (E–H) Single-molecule data simulated from an ideal distribution of 25 nm radius, 10 nm localization precision, and an a/b ratio of either 1.0 or 1.3 at 0, 45, and 90° rotation. While 1,000,000 were used for the simulation, only 1000 are shown here for

ease of visualization. (I–L) 3D density distributions calculated from the data in parts E–H, respectively, with deviations from the ideal radius noted above the 3D density histogram. (M) Summary of a/b ratios ranging from 1.0 to 1.5 using the same simulation parameters as those in parts E–L. figure reprinted with permission from the American Chemical Society [8].

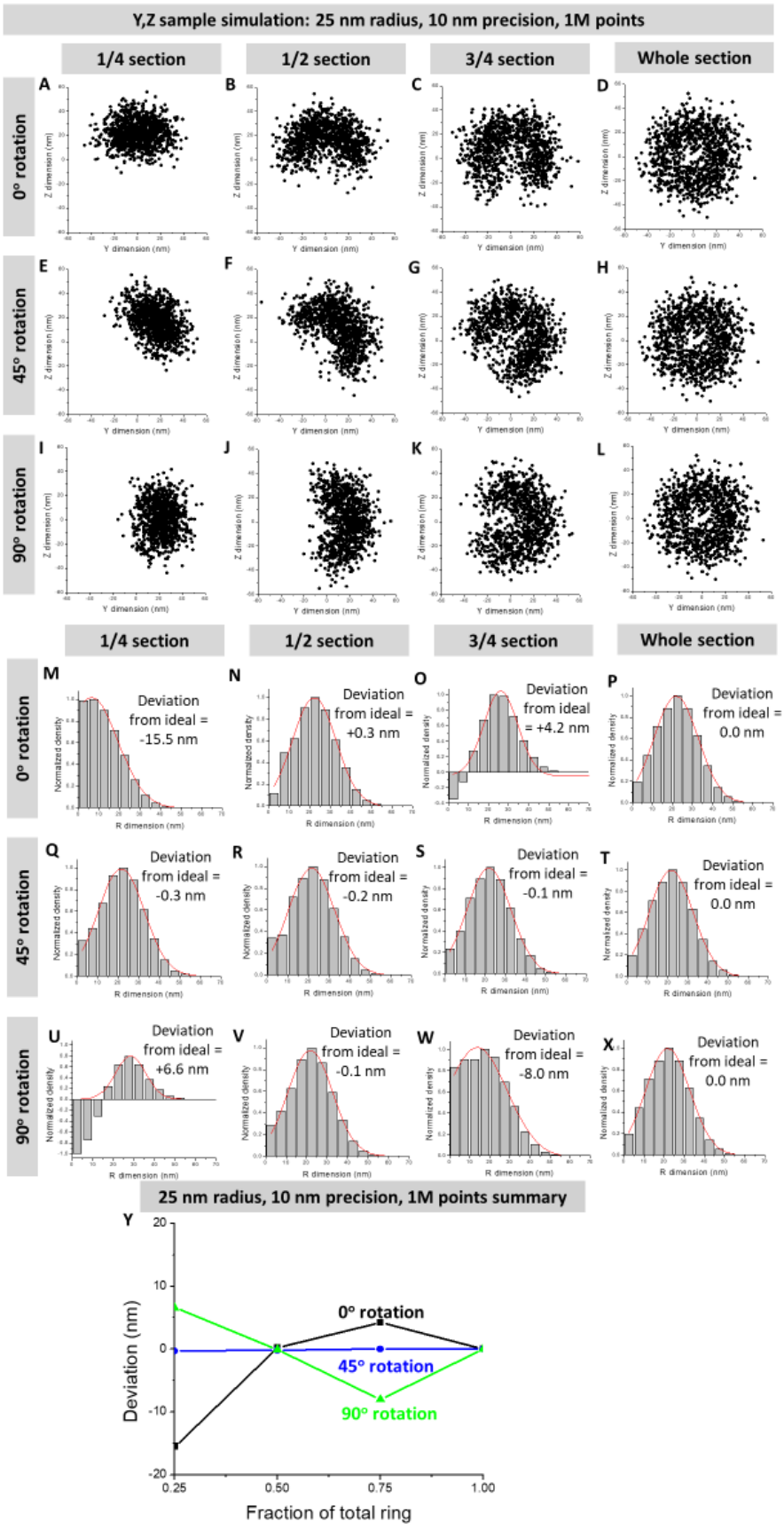
Y,Z sample simulation: 25 nm radius, 10 nm precision, 1M points
1/4 section
1/2 section
3/4 section
Whole section
0° rotation
45° rotation
90° rotation
A
B
C
D
E
F
G
H
I
J
K
L
Z dimension (nm)
Y dimension (nm)
M
N
O
P
Q
R
S
T
U
V
W
X
Deviation from ideal = -15.5 nm
Deviation from ideal = +0.3 nm
Deviation from ideal = +4.2 nm
Deviation from ideal = 0.0 nm
Deviation from ideal = -0.3 nm
Deviation from ideal = -0.2 nm
Deviation from ideal = -0.1 nm
Deviation from ideal = 0.0 nm
Deviation from ideal = +6.6 nm
Deviation from ideal = -0.1 nm
Deviation from ideal = -8.0 nm
Deviation from ideal = 0.0 nm
Normalized density
R dimension (nm)
25 nm radius, 10 nm precision, 1M points summary
Y
Deviation (nm)
Fraction of total ring
0° rotation
45° rotation
90° rotation
20
10
0
-10
-20
0.25
0.50
0.75
1.00

Figure S20 The impact of varying the labeling ratio and rotation is minimal beyond half labeling efficiency. Panels (A)-(D) illustrate simulated single molecule distributions based on an ideal radius of 25 nm, 10 nm localization precision, and different labeling ratios. Despite the simulations comprising 1,000,000 points, only 1,000 are presented here for clarity. Panels (E)-(L) demonstrate simulated rotation angles of 45 and 90 degrees under the conditions described in A-D. Panels (M)-(X) display 3D density histograms derived from A-L, with deviations from the ideal radius indicated above the respective histograms. Panel (Y) summarizes the results obtained from M-X. Figure reproduced with permission[8].

Supplementary Movies 1-21

Movie 1 A 3D view of the POM121 map within the NPC of live cells. The green cloud illustrates the 3D spatial probability density map of POM121's FG-rich terminals, while the light grey structure depicts the NPC scaffold obtained through Cryo-EM and sourced from the RCSB Protein Data Bank. The color bar indicates density, ranging from low (dark) to high (light). Scale bar: 20 nm.

Movie 2 Behold a 3D rendering of the Nup98 map within live cell NPCs. The green cloud showcases the 3D spatial probability density map of Nup98's FG-rich terminals, while the light grey structure represents the NPC scaffold obtained through Cryo-EM and sourced from the RCSB Protein Data Bank. The color bar indicates density, transitioning from low (dark) to high (light). Scale bar: 20 nm.

Movie 3 Presenting a 3D rendering of the Nup62 map within live cell NPCs. The green cloud showcases the 3D spatial probability density map of Nup62's FG-rich terminals, while the light grey structure represents the NPC scaffold obtained through Cryo-EM and sourced from the RCSB Protein Data Bank. The color bar indicates density, transitioning from low (dark) to high (light). Scale bar: 20 nm.

Movie 4 A 3D rendering of the Nup54 map within live cell NPCs. The green cloud showcases the 3D spatial probability density map of Nup54's FG-rich terminals, while the light grey structure represents the NPC scaffold obtained through Cryo-EM and sourced from the RCSB Protein Data Bank. The color bar indicates density, transitioning from low (dark) to high (light). Scale bar: 20 nm.

Movie 5 Behold a 3D rendering of the Nup58C map within live cell NPCs. The green cloud showcases the 3D spatial probability density map of Nup58's FG-rich C terminals, while the light grey structure represents the NPC scaffold obtained through Cryo-EM and sourced from the RCSB Protein Data Bank. The color bar indicates density, transitioning from low (dark) to high (light). Scale bar: 20 nm.

Movie 6 A 3D rendering of the Nup58N map within live cell NPCs. The green cloud showcases the 3D spatial probability density map of Nup58's FG-rich N terminals, while the light grey structure represents the NPC scaffold obtained through Cryo-EM and sourced from the RCSB Protein Data

Bank. The color bar indicates density, transitioning from low (dark) to high (light). Scale bar: 20 nm.

Movie 7 A 3D view of the merged FG-rich terminals of the five FG Nups – POM121, Nup98, Nup62, Nup58, and Nup54 – located at the central scaffold of the NPC in live cells. The green cloud showcases the 3D spatial probability density map of these FG-rich terminals, while the light grey structure represents the NPC scaffold obtained through Cryo-EM and sourced from the RCSB Protein Data Bank. The color bar indicates density, transitioning from low (dark) to high (light). Scale bar: 20 nm.

Movie 8 Behold a 3D rendering of the Nup358 map within live cell NPCs. The red cloud showcases the 3D spatial probability density map of Nup358's FG-rich terminals, while the light grey structure represents the NPC scaffold obtained through Cryo-EM and sourced from the RCSB Protein Data Bank. The color bar indicates density, transitioning from low (dark) to high (light). Scale bar: 20 nm.

Movie 9 A 3D rendering of the hCG1N map within live cell NPCs. The red cloud showcases the 3D spatial probability density map of hCG1's FG-rich N terminals, while the light grey structure represents the NPC scaffold obtained through Cryo-EM and sourced from the RCSB Protein Data Bank. The color bar indicates density, transitioning from low (dark) to high (light). Scale bar: 20 nm.

Movie 10 A 3D rendering of the hCG1C map within live cell NPCs. The red cloud showcases the 3D spatial probability density map of hCG1's FG-rich C terminals, while the light grey structure represents the NPC scaffold obtained through Cryo-EM and sourced from the RCSB Protein Data Bank. The color bar indicates density, transitioning from low (dark) to high (light). Scale bar: 20 nm.

Movie 11 A 3D rendering of the Nup214 map within live cell NPCs. The red cloud showcases the 3D spatial probability density map of Nup214 FG-rich terminals, while the light grey structure represents the NPC scaffold obtained through Cryo-EM and sourced from the RCSB Protein Data Bank. The color bar indicates density, transitioning from low (dark) to high (light). Scale bar: 20 nm.

Movie 12 A 3D view of the merged FG-rich terminals of the three FG Nups – Nup358, hCG1, and

Nup214 – located at the cytoplasmic side of the NPC in live cells. The red cloud showcases the 3D spatial probability density map of these FG-rich terminals, while the light grey structure represents the NPC scaffold obtained through Cryo-EM and sourced from the RCSB Protein Data Bank. The color bar indicates density, transitioning from low (dark) to high (light). Scale bar: 20 nm.

Movie 13 A 3D rendering of the Nup153 map within live cell NPCs. The yellow cloud showcases the 3D spatial probability density map of Nup153 FG-rich terminals, while the light grey structure represents the NPC scaffold obtained through Cryo-EM and sourced from the RCSB Protein Data Bank. The color bar indicates density, transitioning from low (dark) to high (light). Scale bar: 20 nm.

Movie 14 A 3D rendering of the TPR map within live cell NPCs. The yellow cloud showcases the 3D spatial probability density map of TPR FG-rich terminals, while the light grey structure represents the NPC scaffold obtained through Cryo-EM and sourced from the RCSB Protein Data Bank. The color bar indicates density, transitioning from low (dark) to high (light). Scale bar: 20 nm.

Movie 15 A 3D rendering of the Nup50 map within live cell NPCs. The yellow cloud showcases the 3D spatial probability density map of Nup50 FG-rich terminals, while the light grey structure represents the NPC scaffold obtained through Cryo-EM and sourced from the RCSB Protein Data Bank. The color bar indicates density, transitioning from low (dark) to high (light). Scale bar: 20 nm.

Movie 16 A 3D view of the merged FG-rich terminals of the three FG Nups – Nup153, TPR, and Nup50 – located at the nuclear side of the NPC in live cells. The yellow cloud showcases the 3D spatial probability density map of these FG-rich terminals, while the light grey structure represents the NPC scaffold obtained through Cryo-EM and sourced from the RCSB Protein Data Bank. The color bar indicates density, transitioning from low (dark) to high (light). Scale bar: 20 nm.

Movie 17 A 3D view of the transport route of Importin β1 within live cell NPCs. The blue cloud showcases the 3D spatial probability density map of Importin β1, while the light grey structure represents the NPC scaffold obtained through Cryo-EM and sourced from the RCSB Protein Data Bank. The color bar indicates density, transitioning from low (dark) to high (light). Scale bar: 20 nm.

Movie 18 A 3D view of the transport route of CRM1 within live cell NPCs. The blue cloud showcases the 3D spatial probability density map of CRM1, while the light grey structure represents the NPC scaffold obtained through Cryo-EM and sourced from the RCSB Protein Data Bank. The color bar indicates density, transitioning from low (dark) to high (light). Scale bar: 20 nm.

Movie 19 A 3D view of the transport route of TAP/p15 within live cell NPCs. The blue cloud showcases the 3D spatial probability density map of TAP/p15, while the light grey structure represents the NPC scaffold obtained through Cryo-EM and sourced from the RCSB Protein Data Bank. The color bar indicates density, transitioning from low (dark) to high (light). Scale bar: 20 nm.

Movie 20 A 3D view of the passive diffusion route of JF dyes within live cell NPCs. The blue cloud showcases the 3D spatial probability density map of JF dyes, while the light grey structure represents the NPC scaffold obtained through Cryo-EM and sourced from the RCSB Protein Data Bank. The color bar indicates density, transitioning from low (dark) to high (light). Scale bar: 20 nm.

Movie 21 A 3D view of the inhibited passive diffusion of 70-kDa dextran molecules at the cytoplasmic side of the NPC. The blue cloud showcases the 3D spatial probability density map of 70-kDa dextran molecules, while the light grey structure represents the NPC scaffold obtained through Cryo-EM and sourced from the RCSB Protein Data Bank. The color bar indicates density, transitioning from low (dark) to high (light). Scale bar: 20 nm.

References

1. Mukaka, M.M. (2012). Statistics corner: A guide to appropriate use of correlation coefficient in medical research. Malawi Med J *24*, 69-71.
2. Mooney, C.Z. (1997). Monte carlo simulation (Sage).
3. Mahadevan, S. (1997). Monte carlo simulation. Mechanical Engineering-New York and Basel-Marcel Dekker-, 123-146.
4. Ma, J., Goryaynov, A., and Yang, W. (2016). Super-resolution 3D tomography of interactions and competition in the nuclear pore complex. Nature Structural & Molecular Biology *23*, 239-247. 10.1038/nsmb.3174.
5. Ma, J., Goryaynov, A., Sarma, A., and Yang, W. (2012). Self-regulated viscous channel in the nuclear pore complex. Proceedings of the National Academy of Sciences *109*, 7326-7331. doi:10.1073/pnas.1201724109.

6. Mudumbi, K.C., Czapiewski, R., Ruba, A., Junod, S.L., Li, Y., Luo, W., Ngo, C., Ospina, V., Schirmer, E.C., and Yang, W. (2020). Nucleoplasmic signals promote directed transmembrane protein import simultaneously via multiple channels of nuclear pores. Nature Communications *11*, 2184.
7. Li, Y., Aksenova, V., Tingey, M., Yu, J., Ma, P., Arnaoutov, A., Chen, S., Dasso, M., and Yang, W. (2021). Distinct roles of nuclear basket proteins in directing the passage of mRNA through the nuclear pore. Proceedings of the National Academy of Sciences *118*, e2015621118. doi:10.1073/pnas.2015621118.
8. Ruba, A., Luo, W., Kelich, J., Tingey, M., and Yang, W. (2019). 3D tracking-free approach for obtaining 3D super-resolution information in rotationally symmetric biostructures. The Journal of Physical Chemistry B *123*, 5107-5120.